NASA CR-1617

NASA CONTRACTOR REPORT

NASA CR-16

THERMODYNAMIC PROPERTY MEASUREMENTS IN REFLECTED SHOCK AIR PLASMAS AT 12 – 16,000°K

by Allen D. Wood and Kenneth H. Wilson

Prepared by
LOCKHEED MISSILES & SPACE COMPANY
Palo Alto, Calif. 94304
for Ames Research Center

NASA CR-1617

THERMODYNAMIC PROPERTY MEASUREMENTS IN REFLECTED

SHOCK AIR PLASMAS AT   12 - 16,000° K

By Allen D. Wood and Kenneth H. Wilson

CONTENTS

ILLUSTRATIONS

TABLE

INTRODUCTION

The thermodynamic properties of the plasma formed in the reflected shock region of a shock tube were measured over a temperature range of 12,000−16,000°K. These were diagnostic measurements performed to test the measured temperatures against the gasdynamic temperatures computed in the conventional manner from the conservation equations and the equation of state. The results of this effort were essential to clarify the source of a consistent factor of 2 difference between theoretical predictions (based on gasdynamic temperatures) and experimental results for the total radiant intensity of high-temperature air. The total intensity measurements were obtained over the past several years under prior NASA support and have already been reported.[1]

During the preceding contractual year, diagnostic temperature measurements were made between 10,750 and 13,000°K using the following spectroscopic techniques: (1) the integrated line intensity of several NI and OI lines, (2) the shape of H_α, H_β,* and an NI line, and (3) the spectral intensity of the continuum at 4935Å. The experimental techniques and results have been described in considerable detail[2] and the salient features reported in the open literature.[3] The measured temperatures were limited to about 13,000°K because of a rapid loss of accuracy in the results obtained by the first two techniques. This loss resulted from the rapid rise of the continuum relative to the spectral intensity of a line and because the line intensity itself becomes a slowly varying function of temperature.

---

*Hydrogen was present as an impurity in concentrations of a small fraction of 1%.

1

Since measurements were desired to at least 16,000°K to cover the range of the total intensity results, the first task of the present contractual period was to select thermometric techniques that would not suffer a severe loss of high-temperature accuracy and that were relatively straightforward and proven. No measurements involving NI or OI lines in the visible spectral region were suitable and, of the techniques employed last year, only the continuum measurement remained. A careful study led to the decision to add a trace species to the nearly pure air plasma for diagnostic purposes. Hydrogen gas was selected because it is convenient, not unlike air in a thermodynamic sense, and, most important, because it radiates strongly in the visible region via the well-known Balmer series lines.

To avoid reliance on the somewhat uncertain shape[2] of the strongest line (H_α), sufficient hydrogen was added to make the well-known second strongest line (H_β) clearly visible above the air continuum so that its shape could be measured. This required a hydrogen concentration of 10%, but this substantial concentration provided an additional diagnostic technique — a measurement of the Planck function. Because the peak spectral absorption coefficient of H_α is about 30 times that of H_β, a reasonable pathlength could be selected (~ 10 cm) wherein H_α was quite optically thick at its center so that the intensity here was that of the Planck function. At the same time, H_β was nearly optically thin with the important result that neither measurement depended strongly on the precise value of the hydrogen concentration.

The three thermometric techniques used in this work are summarized below:

Diagnostic Technique	Advantages	Disadvantages
Continuum intensity at 4955Å	Almost purely photoelectric; high temperature sensitivity	Total reliance on the work of Morris et al.[4]
Shape of H_β (4861.33Å)	Shape is a well-documented function of electron density; fair temperature sensitivity	Requires time-integrated photographic techniques; becomes quite wide
Planck function at H_α (6562.79Å)	Purely photoelectric; yields temperature directly; requisite radiation constants are very well-known	Low temperature sensitivity; subject to systematic errors

While it is apparent that each of these techniques has disadvantages, they were believed (and are still believed) to be the best diagnostic techniques for the problem at hand. The next chapter discusses the special experimental techniques adopted to minimize these disadvantages while their effect on the accuracy and precision of the measurements will be assessed in the error analyses in a later chapter.

For this experiment the variables used to specify the thermodynamic state of the plasma were temperature, pressure, and concentrations (i.e., mole fractions). The concentrations were assumed rather than measured since, as will be shown, they were relatively unimportant. The remaining variable, pressure, was measured with an endwall pressure gauge in a manner described in the next chapter.

DESCRIPTION OF APPARATUS AND TECHNIQUE

Since much of the apparatus and many of the techniques were similar to those employed last year,[2] the emphasis in this chapter will be on the changes and new techniques.

Spectroscopic Equipment

Two Model 78-000 Jarrell-Ash 1.5 meter Wadsworth Spectrographs were employed: one was used as a conventional spectrograph and the other as a polychromator. The optical systems were unchanged – both created beams about 1.5 mm wide and 10 – 18 mm high across the full diameter of the shock tube. Order-blocking in the spectrograph was done with a Type II UVA Plexiglas filter to clear the first order to above 6700 Å, while in the polychromator, suitable Corning Glass color filters were placed behind each exit slit. So that both instruments could view the same gas at pathlengths less than the full tube diameter, they were located side-by-side on the same side of the shock tube. The beams were concentric in the shock tube and split by a beam splitter located outside the tube window. The beam splitter was a plain glass microscope slide, positioned nearly normal to the emergent beam and arranged so that the transmitted light (~ 90%) was sent to the spectrograph with the remainder sent to the polychromator.

Photomultiplier tubes were placed behind four exit slits in the polychromator. The exit slits were located as follows:

Main Spectral Feature	Center Wavelength (Å)	Full Width (Å)
Continuum	4550	19
Central portion of H_β	4861.3	19
Continuum	5100	19
Planck function at H_α	6562.8	27

4

The reasons behind the choice of the widths will be discussed later. Because the red wing of H_β extended well over the desired continuum wavelength of 4955 Å (this is 95 Å from H_β and half-widths of 75 Å were encountered), the continuum had to be interpolated from data obtained at 4550 and 5100 Å where the contribution from H_β was small (1 − 9%) and where there was no interference from other lines. The intensity at the center of H_β was measured to provide a check on the hydrogen concentration and to assist in the interpretation of the photographic spectra.

Photoelectric Technique

The entire technique of measuring absolute intensities via calibrated photomultiplier (PM) tubes was carefully reviewed with the aim of performing these measurements as accurately as possible. The low temperature sensitivity of the Planck function and the poor PM tube sensitivity at H_α wavelengths motivated this review.

Two basic considerations were involved: first, the signal/noise ratio of a PM tube is proportional to the square root of cathode current divided by frequency bandwidth; and, second, the plasma intensities were up to 10^4 times the intensity of the tungsten-ribbon standard lamp used for calibration. Regarding the second point, one can filter the plasma radiation and/or make the standard lamp appear brighter by opening entrance and exit slits, replacing the beam splitter with a mirror, etc., or one can accept the full magnitude of this disparity. Since filtering the plasma radiation degrades the signal/noise ratio and since the other operations are difficult to do reproducibly, it was decided to accept the full disparity. This meant that linearity was an important consideration. Also the calibration had to be performed under

near-dc conditions because otherwise the signal/noise ratio would be quite low. This was done via an in situ calibration with the standard lamp placed inside the shock tube prior to each shot. The resultant signals were read out on a precision dc microvoltmeter.

To ensure that the PM tube response was linear, the following steps were adopted for the design of each PM tube circuit.

1) The PM tubes were selected for the greatest cathode sensitivity at the wavelengths involved.

2) Based on manufacturers' information and estimates of the radiative flux at the exit slits during the experiment (see ref. 2), the gain and dynode voltage were chosen to cause the peak anode current to be about 20% of the maximum rating.

3) A dynode resistive divider string was designed which drew at least 10^4 times the steady anode current during the calibration.

4) A tapered set of dynode bypass capacitors, designed to deliver the peak current for 25 μsec with less than a 1% change in dynode voltage, was added to the divider string.

5) An anode load resistor (1 kΩ) was chosen to limit the frequency response to 350 kHz (1 μsec rise time) when used with about 15 ft of connecting cable.

To test the design, each PM tube and circuit was driven to nonlinear behavior by using a pulsed xenon flashlamp at various distances under nearly the same illumination (color, cathode area) as in the polychromator. For use in the polychromator, the tubes were always operated at an anode current less than 10% of that value where

6

nonlinear behavior was first noted during this test. These nonlinear points were 1−2 ma and since these were 2−4 times the maximum ratings, it is evident that the above design criteria are consistent with the test results. During use, the output levels were never more than a few tenths of a volt.

Three RCA 1P28/1P21 PM tubes were used for the channels at 4550, 4861, and 5100 Å. For the Planck function measurement at 6563 Å, the flux through the exit slit was split by a half-silvered mirror and sent to two different PM tubes: one a DuMont KM2433 with an S-20 response and the other a Hamamatsu R-136 with a "modified" S-10 response. Each of these tubes was powered by a separate John Fluke power supply so that the precision of the Planck function measurement could be assessed. A third supply powered the three RCA tubes in parallel.

Instrument Standardization

An accurate measurement of the wide shape of H_β required that spectral changes in film sensitivity, instrument transmittance, etc., be taken into account. This procedure is called instrument standardization and it was made difficult because H_β is located in a spectral region where photographic emulsions undergo a rapid change in spectral sensitivity.

To illustrate this, Fig. 1 shows several curves of constant optical density obtained by microdensitometering spectrograms taken of the standard lamp. As in the poly-chromator calibration, the standard lamp was placed in the center of the shock tube and illuminated the spectrograph through the same optics, step wedge, entrance slit,
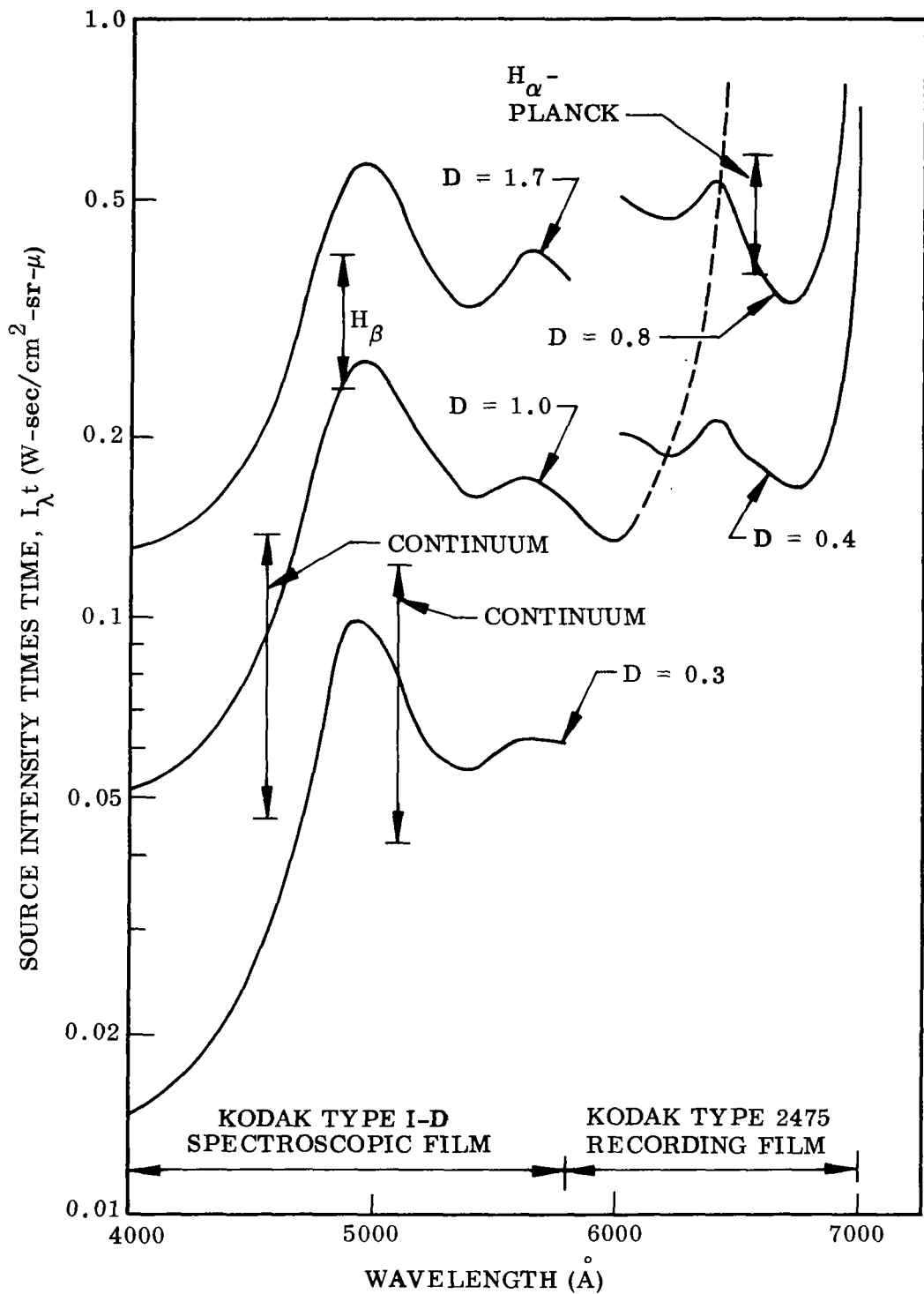
Fig. 1   Constant Optical Density Contours From Spectrograms of
Standard Lamp

etc., as did the plasma. The exposure times were $0.1 - 0.6$ sec and were selected so that the product of lamp spectral intensity and time $(I_\lambda t)$ was comparable to that of the plasma with an exposure time of about 20 μsec. Typical plasma values are shown at the position of the exit slits. If viewed upside down, Fig. 1 would resemble the spectral sensitivity curves supplied by film manufacturers, except that here the ordinate relates to emission at the source rather than energy density at the film.

The most striking feature of this figure is the rapid change at wavelengths near H_β. This is caused by the film as a result of the transition between the response of the silver halide on the blue side to that of the sensitizing dye on the red. The films used in this experiment were Kodak Type I-D Spectroscopic Film for the $3400 - 5800$ Å region and Kodak Type 2475 Recording Film for $5800 - 7000$ Å. The I-D film was chosen because, based on manufacturer's literature, it was supposed to have a fairly uniform response at H_β wavelengths. It turned out that this was not so and, in fact, it was quite comparable to the 2475 film in this respect. It did develop to a high gamma (large difference in density for small difference in $I_\lambda t$) which facilitated the photometric process and so was useful for this reason. Another feature obtainable from Fig. 1 is that the curves at different densities are quite similar which implies that the variations are not particularly density or intensity-dependent.

One measure of the applicability of these curves to the plasma studies is to determine the reciprocity behavior of the films. This was done by obtaining the spectral intensity of the plasma in two ways. One was by the polychromator measurements discussed earlier. The other was a purely photographic process involving two films. The first was known exposure to the standard lamp (~ 0.3 sec) and the second a

9

known exposure to the plasma $(20 - 30 \mu sec)$. Both films were developed simultaneously in the same tank to minimize the variables introduced in the development. Supposedly this left only the reciprocity behavior as the uncontrolled variable. Then by locating points at the same density and wavelength, the plasma intensity could be determined by assuming that reciprocity behavior existed. Examples of the ratio of the polychromatic intensity (averaged over the exposure time) to this purely photographically determined intensity from six such tests are shown by Fig. 2.

Much can be learned from this figure. First, all the points are below the value of unity which would be expected in the absence of reciprocity failure. This implies that reciprocity failure occurred in the 0.3 sec standard lamp exposure which is not at all unreasonable since this time is quite long for these films (reciprocity law failure occurs at both very short and very long exposure times). For any one set of points, the 4550 Å value is within ±10% of the 4861 Å value, while the 5100 Å value differs by several times this amount. This is probably because both 4550 and 4861 Å lie in the silver halide response while 5100 Å lies in the dye response. The 4550 − 4861 Å points cluster about two different values. While the reason for this is unknown, the author suspects that the elapsed time before development may be an important factor. Ordinarily both films were developed shortly after the shot while the standard lamp exposure was taken at least several hours and sometimes as much as 24 hours prior to the shot. Unfortunately records of this nature were not maintained.

The conclusion to be drawn from this effort is that reciprocity behavior cannot be assumed to exist and also that attempting to predict absolute intensities by purely photographic means is quite uncertain even though good photometric technique is
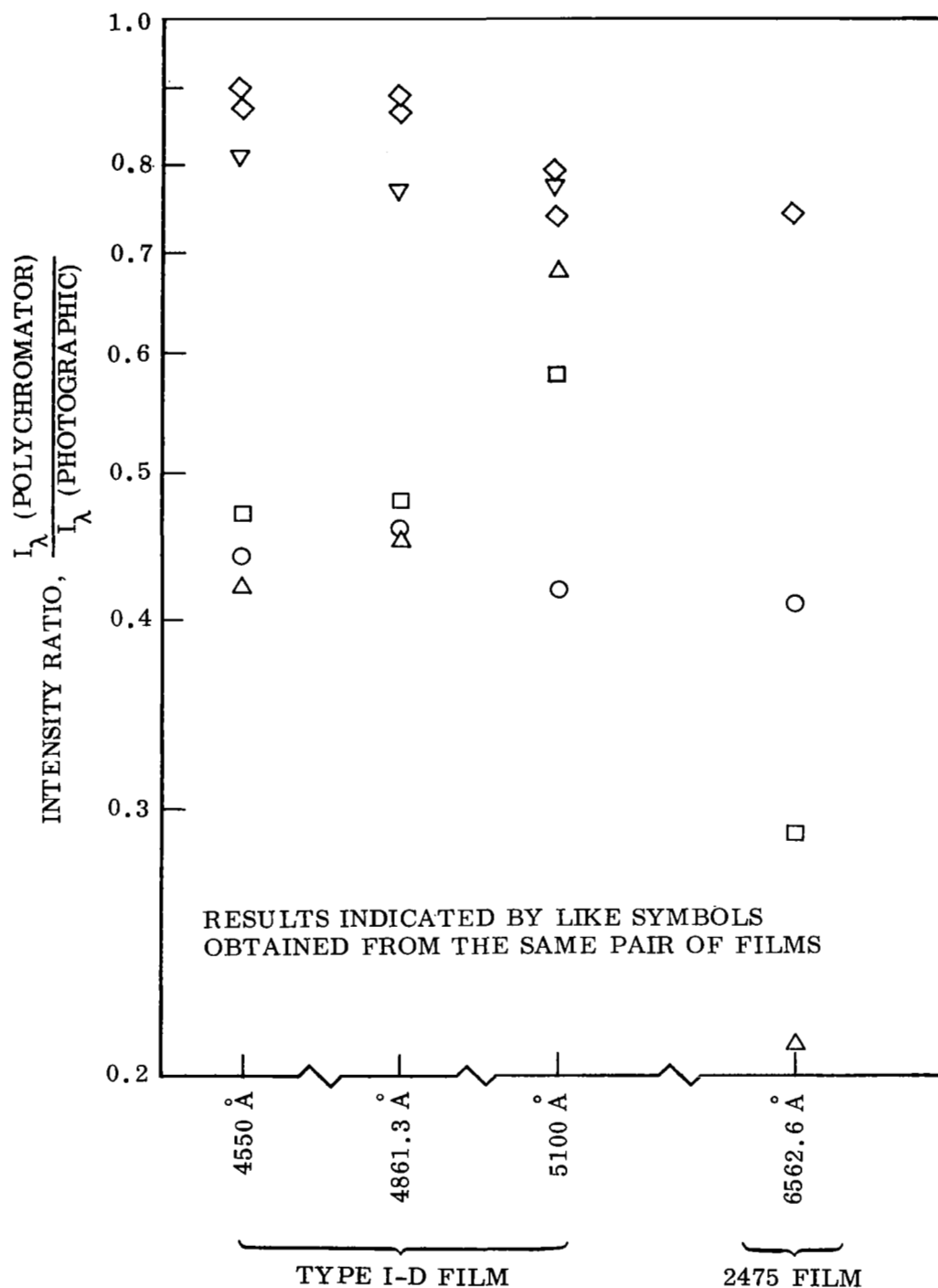
Fig. 2 Results From Six Attempts To Determine Plasma Intensities by Purely Photographic Methods (Neglecting Reciprocity Effects)

11

practiced. The plasma/standard lamp intensity ratio of 10^4, or the exposure time ratio of 10^{-4}, is too great. In retrospect a factor of 10 decrease in the standard lamp exposure time done, say, by opening the entrance slit 10×, may have overcome much of the reciprocity law failure. However this was not important for this experiment.

The instrument standardization technique adopted for this experiment embraced the above observations concerning the film behavior. It avoided any dependence on the reciprocity law and utilized (but did not depend on) the similarity of the constant-density curves of Fig. 1. Briefly this technique forced the photographically determined line shape to fit the polychromatic intensities of 4550, 4861, and 5100 Å and to follow the trends shown on Fig. 1 at intermediate wavelengths.

The process of accomplishing this began with the basic standardization curve shown by Fig. 3. The ordinate is called the k-factor defined by:

$$k(\lambda) = \frac{(I_\lambda t) \text{ from standard lamp to give a density D at } \lambda}{(I_\lambda t) \text{ from standard lamp to give same density at } 4861 \text{ Å}} \tag{1}$$

This basic curve could be obtained from any of the curves of Fig. 1 by dividing by the appropriate normalizing factor. In fact it represents an average of several such curves obtained at densities near unity although the resultant curve is not considered to be a strong function of density because of the similarity discussed above.

The other important ingredient was the density-log exposure curve (the H-D curve)* obtained from the actual spectrogram at the brightest spectral feature — the maximum

---

*This curve was obtained from the actual spectrogram through the use of a step wedge at the entrance slit of the stigmatic Wadsworth spectrograph. Complete details of this technique are given in Ref. 2.
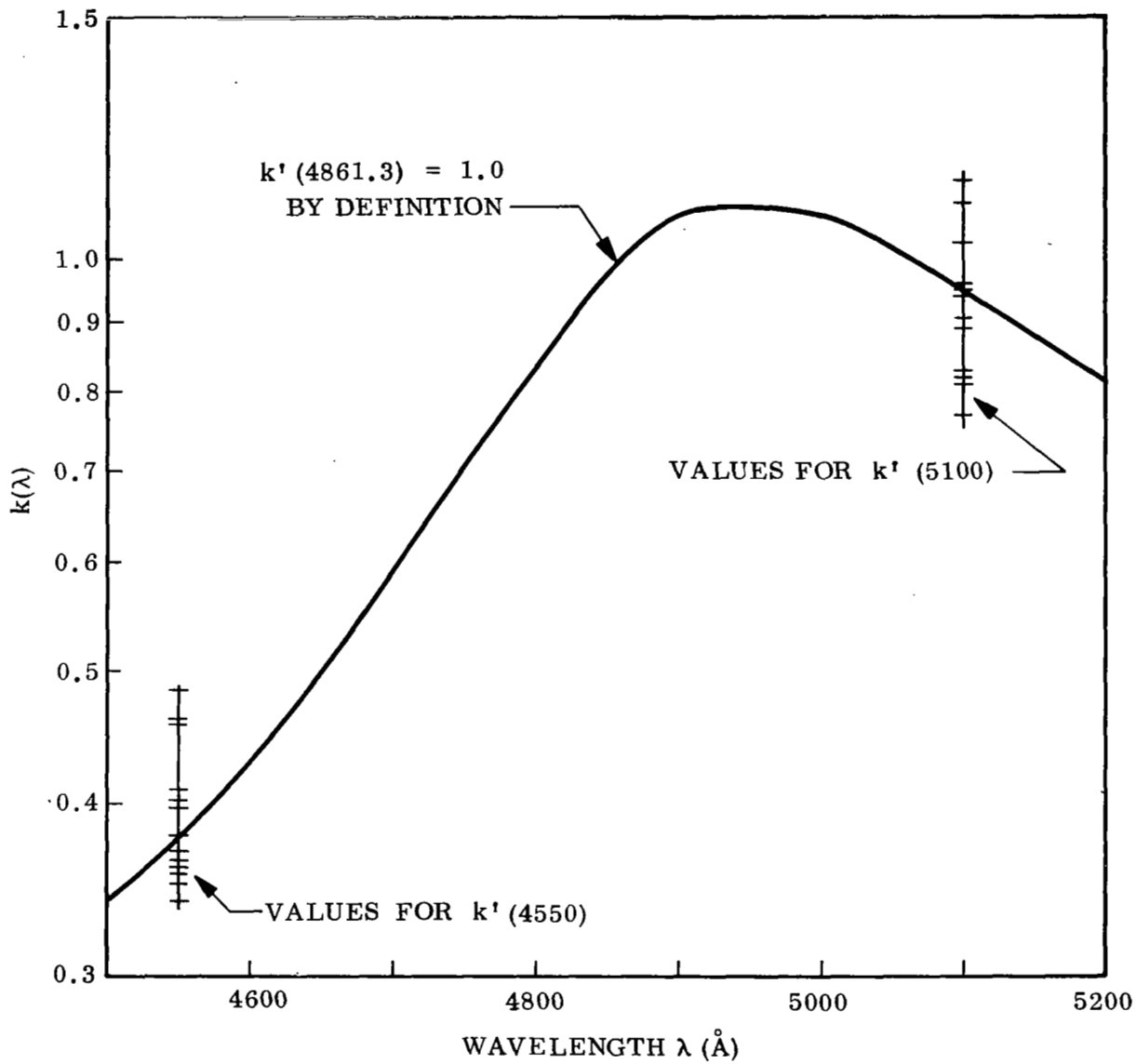
Fig. 3 Basic Standardization Curve for Wavelengths About H_β

of the blue wing of H_β at $4840 - 50$ Å. A value of 100% relative exposure was assigned to this feature following standard photometric technique.[2] Again because of the similarity discussed above, this curve is not considered to be a strong function of wavelength.

The equation used to obtain the spectral intensity at any wavelength near H_β was

$$I_\lambda(\lambda) = [I_{\lambda o}(H_\beta)] \times k'(\lambda) \times [H-D] \qquad (2)$$

The last factor, $[H-D]$, refers to the relative exposure at the density of the point of interest as obtained from the H-D curve in the standard way. The first factor, the normalizing constant, was obtained by solving the above equation on the average for the 19 Å region about 4861.3 Å corresponding to the H_β exit slit. Here the k-factor is about unity with the result that the average value of the last two factors was about 0.90 (the actual shape of H_β was used here as opposed to the theoretical shape as discussed later). Then, by inserting the polychromatic intensity on the left-hand side, the above equation was solved for the normalizing constant $[I_{\lambda o}(H_\beta)]$.

The process of forcing the line shape to fit the polychromatic intensities was accomplished by solving Eq. (2) at 4550 and 5100 Å for the k' factors. Because these were continuum channels, no averaging was required. These two k' factors generally lay near, but not upon, the basic standardization curve (Fig. 3) because of the various approximations involved. The range of these k' values, for all 16 shots of this experiment, is shown on Fig. 3. The procedure then was to modify this basic curve by fairing in a smooth curve between the three k' values $[k'(H_\beta) = 1.0$ by definition] with due regard to the wavelength dependence of the basic curve. The procedure adopted for this fairing was to make the deviation between these curves linearly

proportional to the distance away from 4861 Å. Then Eq. (2) was used with this new k' curve to obtain the entire shape between 4550 and 5100 Å. Thus, this standardization technique forced the resultant shape to fit the relatively well-known polychromatic intensities, utilized the actual H-D curve, and accounted for spectral changes in the film sensitivity, instrument transmittance, etc., in a realistic manner.

A somewhat similar procedure was followed for the red region where H_α was located. Since only one polychromator exit slit was used, only the normalizing intensity could be obtained and the standardization curve (derivable from Fig. 1) was used without any fairing process. This was not a serious disadvantage because, as will be shown later, the shape of the optically thick H_α line was not essential to this experiment.

Gas Mixing and Tube Loading Procedure

Because of the explosive nature of an air-hydrogen mixture, each mixture was individually prepared in a small container by loading from a manifold system connecting bottles of air and hydrogen. The container was filled to a predetermined total pressure of 45.5 Torr and the contents were then dumped into the evacuated shock tube with gas flow allowed for 1 min, after which the tube was isolated. The resultant initial shock tube pressure of 0.206 Torr was measured on several occasions with a calibrated McLeod gauge (a Todd Scientific Co. Universal Vacuum Gauge).

This calibration was done by admitting known volumes of room air into the evacuated shock tube and calculating the pressure through Boyle's law and the known tube volume. These pressures were about 1% above the values measured by a precision manometer (a Datametrics Inc. Barocel Electronic Manometer) and this agreeement is taken as verification of the calculated pressure.

The calibration revealed that the McLeod gauge read 8% high at pressures about 0.2 Torr, caused at least in part by an incorrect capillary correction designed into the instrument scale. This rather significant calibration correction was not discovered until nearly the end of the experimental period during an effort to reconcile the measured endwall pressures (discussed next) with the gasdynamic pressures. This report, of course, reflects this correction but since this same gauge was used to determine initial pressures in the past, the same cannot be said for prior reports and publications.[1,2,3] The significance of an initial pressure too high by 8% will be discussed in the appropriate places in this report.

Pressure Measurements

The other measured thermodynamic variable — pressure — was obtained via a pressure transducer installed flush with the endwall about 38 mm from the tube wall and slightly outside the field of view of the optical instrumentation.

Two different kinds of pressure transducers were employed during the course of the experiment. One was a Kistler Instrument Corporation Model 603A (0 − 3000 psi, 0.35 pcb/psi, 500 kHz) and the other a pcb Piezotronics, Inc., Model 102A12 (vacuum to 100 psi, 20 mV/psi, 500 kHz) transducer. Both gauges were calibrated in a special apparatus which utilized a dynamic process starting with a vacuum.

To demonstrate the nature of the resultant endwall pressure signals, some of the traces obtained with the pcb Piezotronics gauge are shown on Fig. 4. Also shown are the computed gasdynamic pressures, and it is clear that the two values are in good

agreement. The results obtained with both transducers, which will be shown later, indicated that the measured values were within $\pm 3\%$ of the gasdynamic pressure. The gasdynamic value was used in the thermometric data reduction, and the significance of the $\pm 3\%$ uncertainty will be discussed in the error analyses of the next chapter.

PRESSURE (atm)

SHOT NO. 628
U_s = 10.26 mm/μs

SHOT NO. 630
U_s = 9.51 mm/μs

SHOT NO. 631
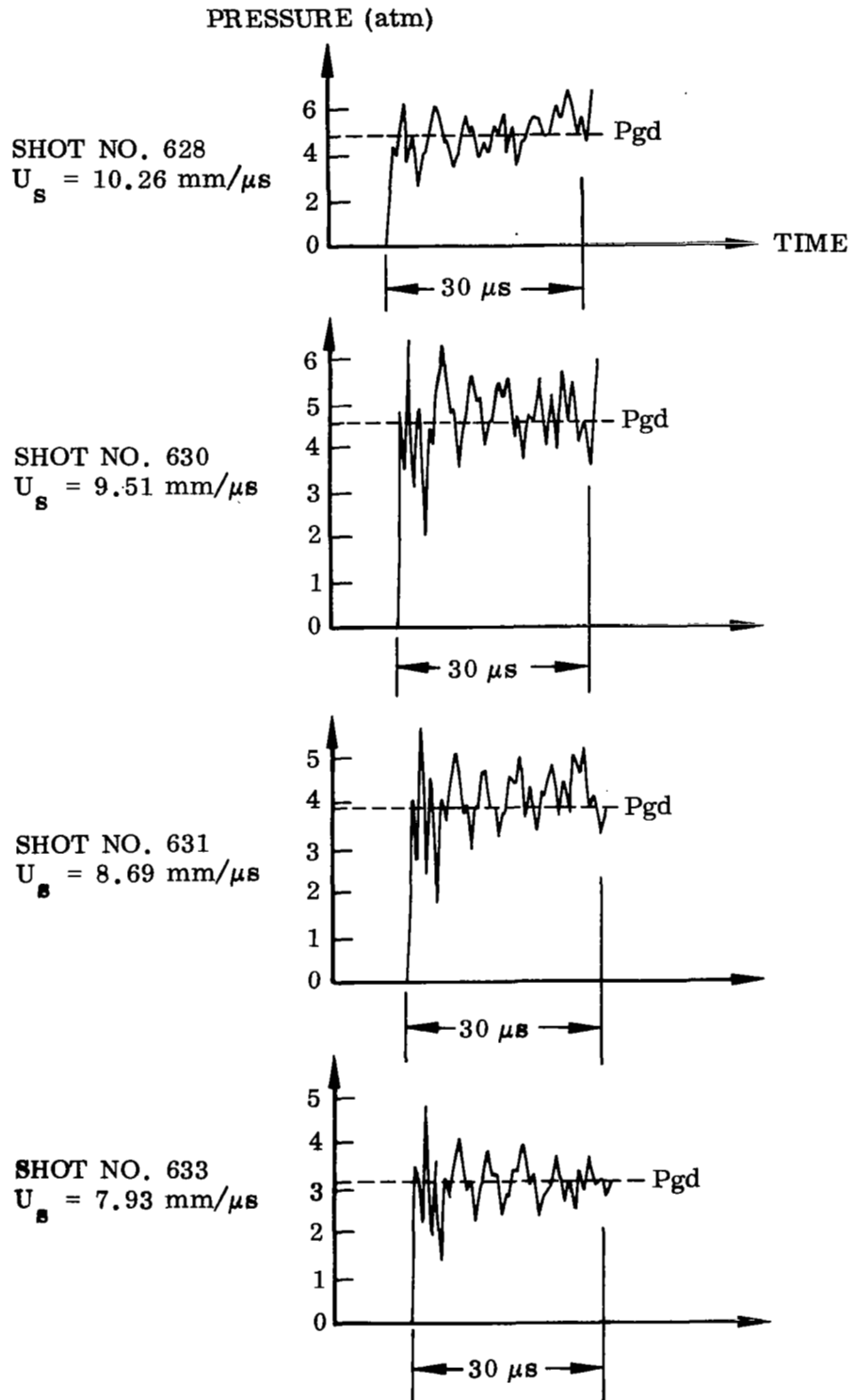U_s = 8.69 mm/μs

SHOT NO. 633
U_s = 7.93 mm/μs

Fig. 4 Examples of Endwall Pressure-Time Histories
Obtained With Piezotronics Pressure Transducer

18

PLASMA THERMOMETRY

Computation of Gasdynamic Properties

The gasdynamic temperatures and pressures provide the basis of comparison through-out this report and thus it is appropriate to discuss how they were obtained. To begin, the conservation equations will be written in a simple form without involving the equation of state.

Applying the equations for conservation of mass, momentum, and energy across the incident shock wave and eliminating the particle velocity leads to

$$P_2 - P_1 = \rho_1 U_s^2 [1 - (\rho_1/\rho_2)] \tag{3}$$

$$H_2 - H_1 = \frac{1}{2} U_s^2 [1 - (\rho_1/\rho_2)]^2 \tag{4}$$

Since for the conditions of interest the density ratio is about 17 (i.e., $\rho_2 = 17\rho_1$), it is clear that the pressure and enthalpy behind the incident shock are only weakly dependent on the density ratio and hence the equation of state.

The result of a similar analysis for the reflected shock is

$$P_5 - P_1 = \rho_2 U_s^2 f(\rho) \tag{5}$$

$$H_5 - H_1 = U_s^2 f(\rho) \tag{6}$$

where

$$f(\rho) = \frac{[1 - (\rho_1/\rho_2)]}{[1 - (\rho_2/\rho_5)]} \left(1 - \frac{\rho_1}{\rho_5}\right)$$

19

Here density ratios of about 8 ($\rho_5 = 8\rho_2$) are typical. While the enthalpy retains its weak dependence on the density ratio, the pressure does not because of the linear ρ_2 factor. Thus the reflected shock enthalpy is only weakly dependent on the equation of state while the reflected shock pressure is linearly dependent on the density ρ_2 and hence the equation of state as applied to the gas behind the incident shock.

An equation of state, in the form $\rho = f(P, H)$, was obtained from a LMSC free-energy minimization program called FEMP. FEMP requires thermodynamic data in the form of curve fits to tabulated values of free energy and entropy for the components considered ($N_2, N, N^+, O, O^+, H, H^+$, and e^-). The data for air were taken from Gilmore[5] and for hydrogen, from McBride.[6] Four sets of curve-fit coefficients were used to cover the range $6,000 - 18,000°K$ so that these curve fits would closely approximate the tabulated data. To test FEMP, it was run for pure air at near-gasdynamic conditions of T, P which corresponded to those of the tabulated composition data by Hilsenrath and Beckett.[7] The FEMP values were very close — enthalpy and density to 0.05%, electron density typically 0.2% with 0.6% maximum, and individual species concentrations better than the electron concentrations. Although no composition data were available to check the air + 10% hydrogen mixture, the same mathematics were employed and there is every reason to believe that the results would be equally good.

Given elemental composition and temperature and pressure, FEMP can compute the remaining properties directly, but the gasdynamic variables of enthalpy and pressure require an iterative solution. Since the gasdynamic equations themselves are implicit in density, a computation of shock states requires a double iteration. The entire shock calculation program was analyzed and the convergence criteria for

20

densities and enthalpies set at 0.01% to make the output as good or better than the original thermodynamic data. Table I contains a sampling of the computed gasdynamic states for the reflected shock region which cover the range of this experiment.

Besides being used for the gasdynamic calculation, FEMP provided data at "even" temperatures and pressures for use in calculating the partial derivatives required in the error analyses which follow, for use in obtaining temperature from electron density and pressure, and for deriving approximate equations of state.

One practical use of the latter is to consider the effect on the reflected shock temperature if the initial pressure used in the computation was 8% high. From Eqs. (5) and (6), it is clear that H_5 would be virtually unchanged and that P_5 would be high by 8% because of its dependence on ρ_2. The appropriate form of the equation of state is $T = k(P)^{0.04 - 0.06} (H)^{0.8 - 0.4}$ for the conditions of interest. Hence raising P_1 by 8% would raise the reflected shock temperature by only $0.3 - 0.5\%$.

To determine the sensitivity of the gasdynamic temperature to the hydrogen concentration, temperatures were computed for various concentrations with P_1 and U_s held fixed. The results showed a 60°K decrease in temperature for each 1% of hydrogen added. Thus a 10% error in the hydrogen concentration would affect the gasdynamic temperature by about 0.5% and hence accuracy in the hydrogen concentration was not of paramount importance.

Hydrogen Seeding

The reasoning behind the decision to seed the plasma with hydrogen has already been discussed in the Introduction. The experimental requirements for the hydrogen diagnostic measurements were 1) that H_β be fairly optically thin and have a peak

Table 1

COMPUTED GASDYNAMIC STATES FOR THE REFLECTED SHOCK REGION

T_1 = 294° K
P_1 = 0.206 Torr
H_1 = 77.9 Cal/g
ρ_1 = 2.94^{-7} g/cc

Species	Mole Fraction	Mass Fraction	Gram–Atom Ratio
H_2	0.100	0.0077	0.7643
O_2	0.189	0.2311	1.444
N_2	0.711	0.7612	5.434

U_s (mm/μsec)	T_5 (°K)	P_5 (atm)	ρ_5 (g/cc)	H_5 (cal/g)	Number Densities (particles/cm³)							
					e	N	O	H	N^+	O^+	H^+	N_2
7.8	12,519	3.081	3.596^{-5}	1.568^{+4}	1.52^{+17}	1.06^{+18}	2.93^{+17}	1.54^{+17}	1.20^{+17}	1.99^{+16}	1.13^{+16}	7.45^{+14}
8.0	12,910	3.285	3.650^{-5}	1.650^{+4}	1.88^{+17}	1.04^{+18}	2.93^{+17}	1.54^{+17}	1.49^{+17}	2.48^{+16}	1.39^{+16}	5.48^{+14}
8.2	13,275	3.490	3.700^{-5}	1.734^{+4}	2.27^{+17}	1.03^{+18}	2.92^{+17}	1.54^{+17}	1.80^{+17}	3.01^{+16}	1.68^{+16}	4.16^{+14}
8.4	13,617	3.693	3.744^{-5}	1.819^{+4}	2.68^{+17}	1.01^{+18}	2.90^{+17}	1.52^{+17}	2.12^{+17}	3.57^{+16}	1.98^{+16}	3.21^{+14}
8.6	13,941	3.892	3.778^{-5}	1.906^{+4}	3.10^{+17}	9.91^{+17}	2.87^{+17}	1.51^{+17}	2.46^{+17}	4.17^{+16}	2.30^{+16}	2.52^{+14}
8.8	14,265	4.082	3.792^{-5}	1.996^{+4}	3.55^{+17}	9.61^{+17}	2.82^{+17}	1.48^{+17}	2.80^{+17}	4.82^{+16}	2.64^{+16}	1.96^{+14}
9.2	14,829	4.394	3.774^{-5}	2.176^{+4}	4.38^{+17}	8.91^{+17}	2.68^{+17}	1.41^{+17}	3.44^{+17}	6.06^{+16}	3.29^{+16}	1.23^{+14}
9.6	15,327	4.575	3.656^{-5}	2.358^{+4}	5.08^{+17}	7.99^{+17}	2.46^{+17}	1.30^{+17}	3.98^{+17}	7.20^{+16}	3.86^{+16}	—
10.0	15,814	4.766	3.548^{-5}	2.549^{+4}	5.79^{+17}	7.11^{+17}	2.25^{+17}	1.19^{+17}	4.50^{+17}	8.39^{+16}	4.46^{+16}	—
10.4	16,335	5.078	3.517^{-5}	2.751^{+4}	6.63^{+17}	6.39^{+17}	2.07^{+17}	1.10^{+17}	5.12^{+17}	9.86^{+16}	5.20^{+16}	—

Note: $a.bc^{\pm y}$ = $a.bc \times 10^{\pm y}$.

spectral intensity at least equal to that of the underlying air continuum and 2) that H_α be reasonably optically thick over a spectral interval wide enough to permit an unambiguous measurement of the Planck function. The experimental variables were the amount of hydrogen added and the test gas pathlength. Fortunately, because of the nature of the hydrogen lines, all these experimental requirements could be met.

This is shown by Fig. 5 which was drawn for the air + 10% hydrogen mixture. While a 10% concentration is admittedly a fairly substantial seeding concentration, it is clear from the figure that this amount was required to keep the H_β/continuum intensity ratio above unity at the higher temperatures. The shaded area denotes the operating region where ϵ_β, the maximum emissivity at H_β (peak line + continuum), is about 0.3 while ϵ_α, the maximum emissivity at H_α (considering only the line), is about 0.999. Pathlengths of 12 and 8.5 cm were used in this experiment and the lowest shock velocity was 7.9 mm/μsec. A shape measurement is independent of the absolute intensity provided that the line is optically thin and a peak emissivity of 0.3 is reasonably close to this. For H_α, the considerations become more complicated and involve the width of the exit slit.

H_α-Planck Function Measurement

A rather wide exit slit was desirable for this measurement for two reasons. First, the low cathode sensitivity at 6563 Å of even red-sensitive photomultiplier tubes dictated that the incident light flux be high to obtain a good signal/noise ratio. Second, a wide exit slit would minimize a possible correction for boundary layer absorption at the line center. (There was evidence of this on some preliminary spectograms taken at different conditions and so the H_α shape was monitored during the experiment for this reason, but no further evidence of boundary layer absorption was found.) On
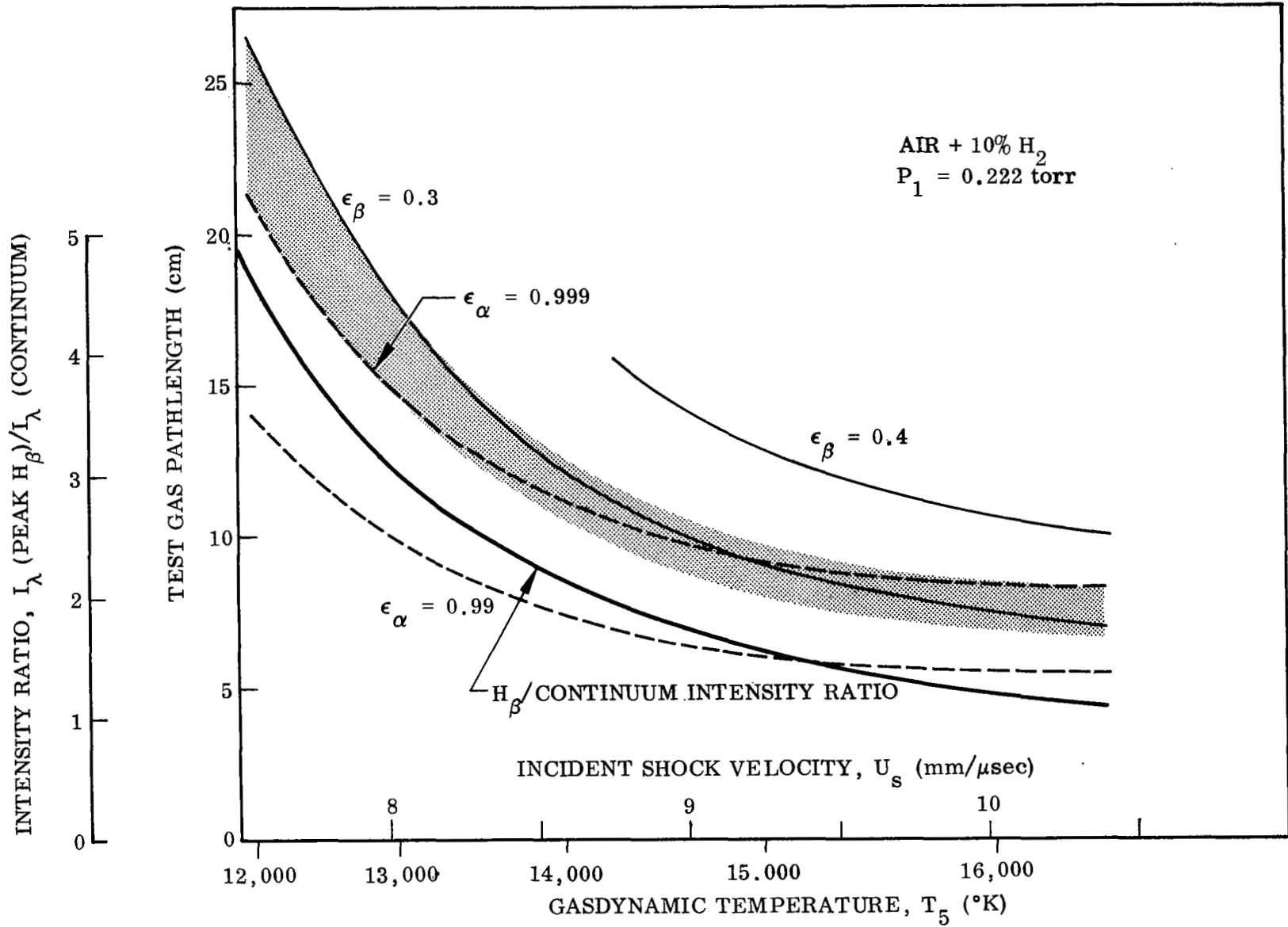
Fig. 5 Operating Region for Best Hydrogen Diagnostics

the other hand a wide exit slit means that the measured intensity (which is an average value) is not the Planck function and hence a correction for this must be applied. Since this correction is uncertain and there is little room for error in this diagnostic measurement, it should be kept small and this means a narrow exit slit. Thus a compromise had to be made. The following table, prepared using the H_α line shapes of Kepple,[8] was used to select the 27Å exit slit.

Electron Density	Maximum Emissivity	Emissivity at $\lambda - \lambda_o = \pm 13.5$Å	Planck Function Correction
1×10^{17}	0.99	0.57	~20%
1×10^{17}	0.999	0.72	~10%
2×10^{17}	0.99	0.76	~10%
2×10^{17}	0.999	0.89	~ 3%

These electron densities are on the low side of the range encountered during this experiment and the tabulated values are conservative in that the continuum and wings of other lines were not included. This thermometer was not used if the experimentally determined correction was over 10% and this happened on only one shot — the slowest. It was 8% on the next slowest and below 4% for the remainder, while no correction was necessary for the seven fastest shots.

H_β Halfwidth Measurement

The determination of the H_β halfwidth was complicated by asymmetries in the measured shapes — the blue peaks were higher than the red ones and the central minimum points shifted several Angstroms toward the red from 4861.33Å. These features have been noted by Kitaeva and Sobolev[9] among others and so it is felt that

they are real and not caused by an incorrect instrument standardization process. Many experimenters symmetrize a measured shape by averaging the two wings, but this was inconvenient in our case. Attempts to asymmetrize the theoretical shapes using Griem's[10] prescription (Eq. 4-96) were unsuccessful — the correction increased linearly toward the wings while just the opposite effect appeared warranted.

A practical solution, suggested by Hill[11] and adopted for this experiment, was to measure the halfwidths* of the blue and red wings separately, average the results, and determine the electron density from this average and the halfwidth tabulations of Kepple.[8] This meant abandoning the concept of fitting an entire line shape as employed last year,[2] but this concept loses significance when unknown asymmetries are present. In addition, the instrumental halfwidth of $0.29\,\text{Å}$ was negligibly narrow so no computer-aided convolutions were required.

Obtaining the average halfwidth was not without its difficulties as typified by Fig. 6 for the shot with the highest incident shock velocity. This spectrum includes more than H_β and the continuum: the ever-present, untabulated NI multiplet at $4630 - 4680\,\text{Å}$ caused little difficulty, but the NI^9 multiplet $(4915, 4935\,\text{Å})$ often lay over the half-intensity point of the red wing. Also both H_β wings extend over the 4550 and $5100\,\text{Å}$ polychromator channels and complicate the determination of the continuum. This figure clearly shows the factors influencing the location of these channels to measure the continuum at $4955\,\text{Å}$. To demonstrate the asymmetries, the theoretical H_β shape from Kepple[8] at the experimental conditions is superimposed. The under-prediction of the central minimum point is commonly known and, except for a wave-length shift, the theoretical shape looks reasonable at the half-intensity points.

---

*The halfwidths are defined here as the intervals between the half optical depth wave-lengths of each wing and $4861.3\,\text{Å}$, with each wing treated separately.
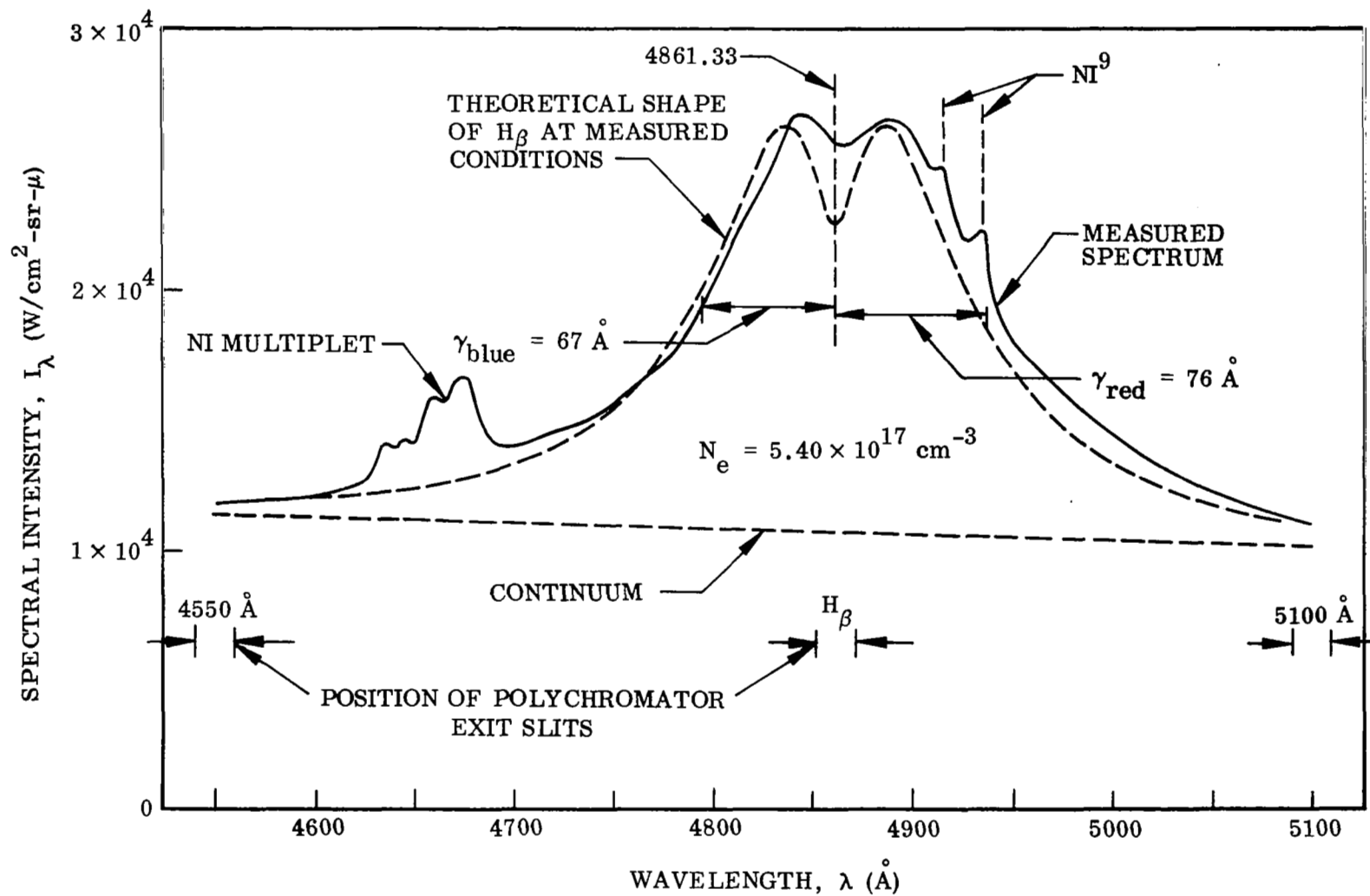
Fig. 6 4550−5100 Å Spectrum From Shot 629 (U_s = 10.35 mm/μsec)

The data reduction procedure used to measure the halfwidths was iterative, but an educated initial guess of the temperature and the corresponding (see below) electron density minimized this problem. Because the measured spectrum was on an absolute basis, the contribution of the NI[9] multiplet could be determined and subtracted off. This was at most a 7% correction since the multiplet peaks were avoided. The continuum levels at 4550 and 5100 Å were determined by subtracting off the wings of H_β obtained from either the tabulated shape or, at lower electron densities, the asymptotic wing formula also tabulated by Kepple.[8] Since this wing correction depended on the height of H_β which in turn depended on the continuum level, a secondary iteration was required. This was done carefully since it affected the continuum level which was important in its own right. This was at most a 9% correction, but it was never less than 1% because the wings extend quite far and the relative height of H_β increased at lower temperatures. (See Fig. 5.) Both this and the NI[9] correction were facilitated by the advance preparation of curves for the NI[9] multiplet intensity at various wavelengths and the H_β wing at 4550 and 5100 Å evaluated along the Hugoniot states.

The red and blue halfwidths were then measured relative to λ_o = 4861.3 A which is unimportant if they are averaged, but later their ratio will be used to estimate the experimental precision. Since peak emissivities of about 0.35 were encountered, opacity effects were taken into account by measuring the halfwidths at the half-optical depth points rather than the half-intensity points. This was done by converting the peak and continuum intensities into optical depths, calculating the half-optical depths, and converting these back into intensities which were then plotted on the spectrum as shown. These differ in Fig. 6 because the blue peak and the blue

continuum were higher. The two halfwidths were then averaged to yield $\bar{\gamma}$ and the electron density calculated from

$$\bar{\gamma} = 1.25 \times 10^{-9} (N_e) \alpha_{1/2} \tag{7}$$

The value of $\alpha_{1/2}$ was obtained from the halfwidth tabulations of Kepple[8] by interpolating between N_e and T for values along the shock Hugoniot. It was constant $(\alpha_{1/2} = 0.0865)$ to better than 1% for this particular path.

Examination of the FEMP tabulations for air + 10% H_2 at "even" temperatures and pressures (which were varied in a stair-step manner along the Hugoniot) revealed that the pressure dependence of the electron density was adequately described by $N_e = k P^{0.6} f(T)$. Therefore a curve of $N_e/P^{0.6}$ vs T was prepared to obtain a temperature from the H_β electron density and the gasdynamic pressure. Finally this temperature was compared with the guessed value to determine whether a second iteration was necessary, but an initial guess of 0.95 T_{gd} was usually adequate.

An example of the measured and theoretical shapes at one of the lower electron densities is shown by Fig. 7. Here the asymmetries are less pronounced but still quite apparent near the line center. The two shapes lie very close to each other near the half-optical depth points, but since these are different, the red halfwidth is still greater than the blue.

The ratio of the two halfwidths ($\gamma_{blue}/\gamma_{red}$) and the ratio of the intensities of the two peaks were plotted against electron density in Fig. 8. There are few if any trends in
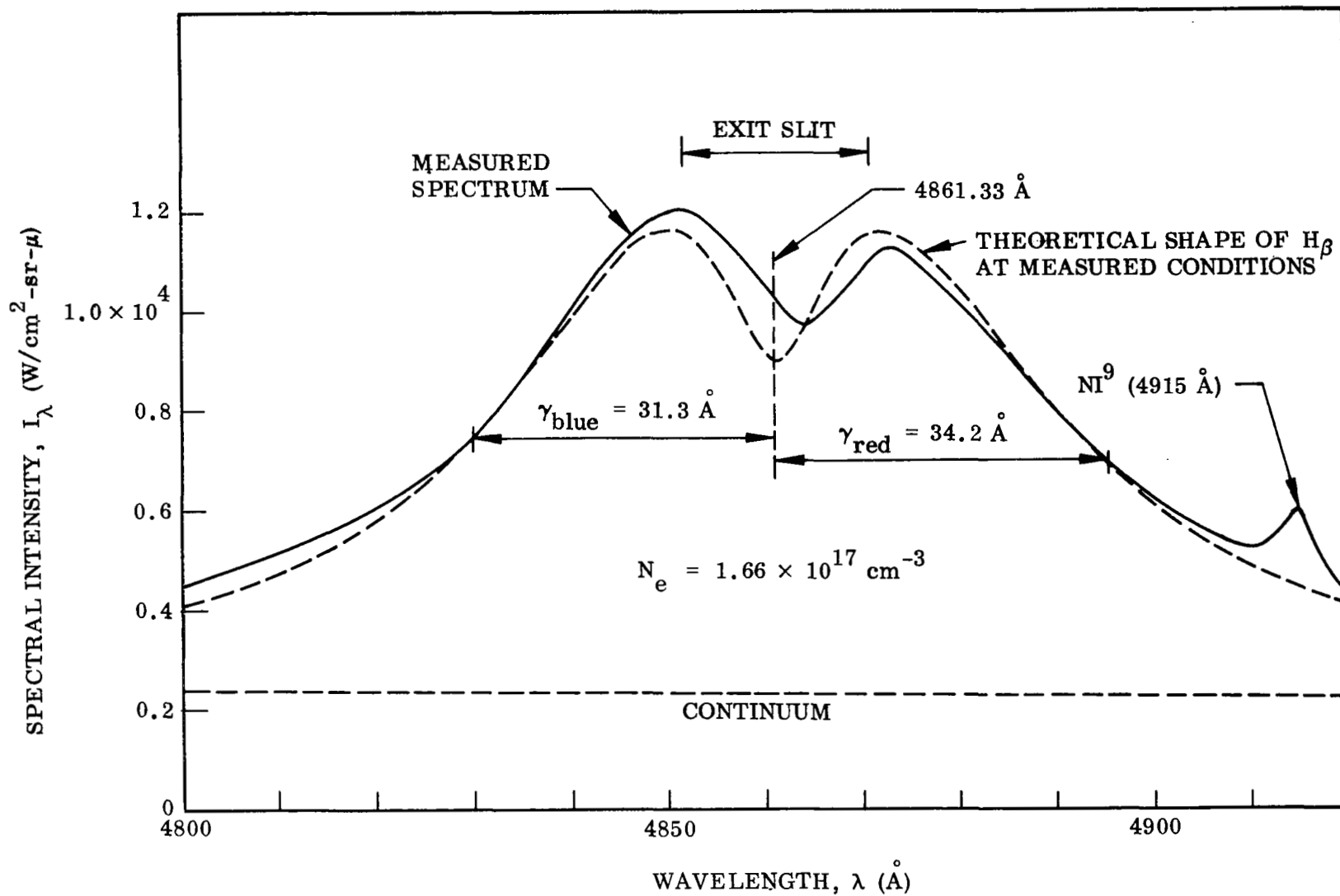
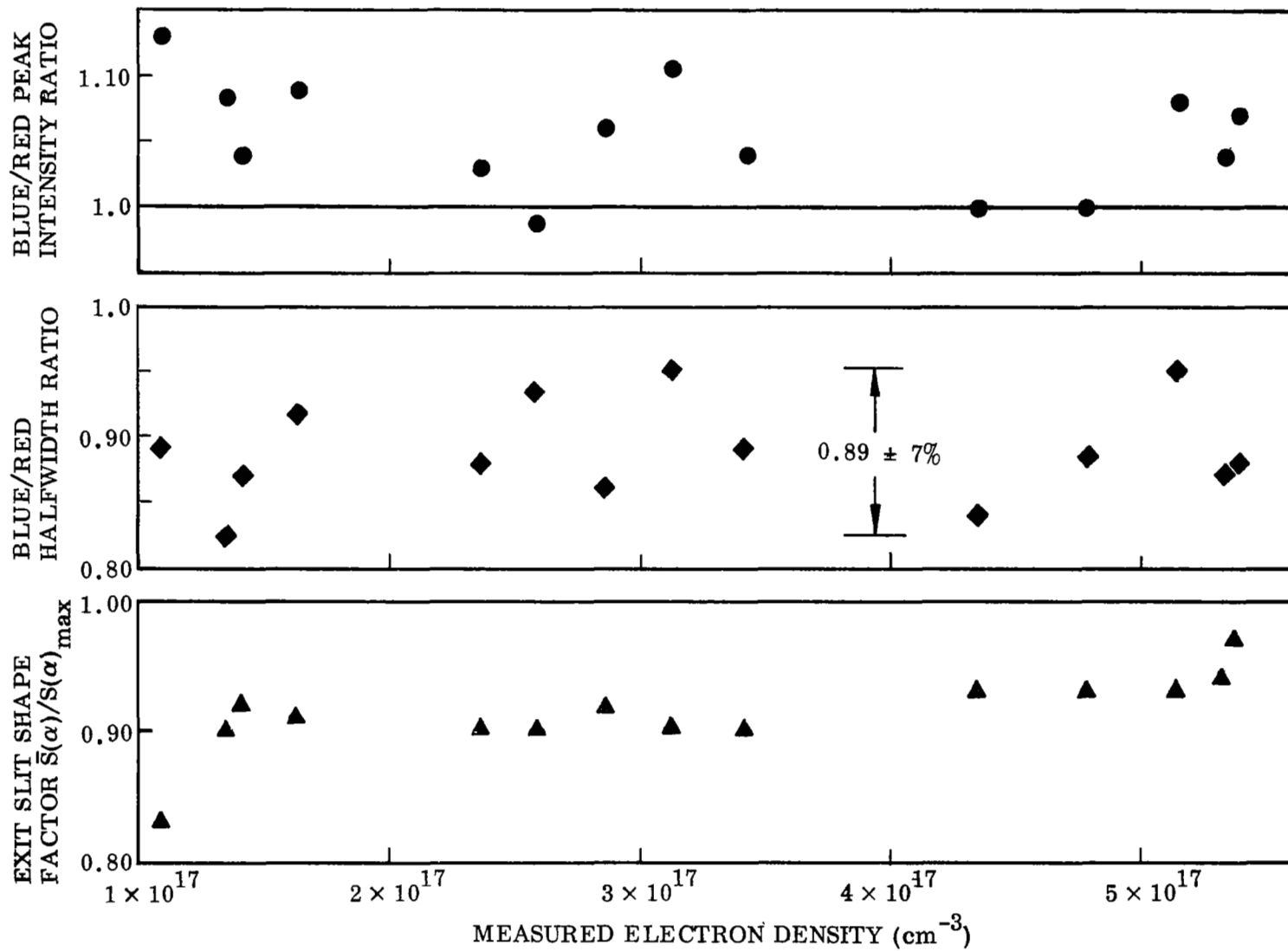Fig. 7 4800 − 4920 Å Spectrum From Shot 619 (U_s = 7.97 mm/μsec)

Fig. 8 Data From the H_{β} Shape Measurements

these ratios, so the fact that the halfwidth ratios vary by $\pm 7\%$ provides an estimate of the experimental precision in this measurement. The lower curve of Fig. 8 represents the ratio of the average spectral intensity of H_β over the 19 Å exit slit width to the average peak spectral intensity of the line. This ratio will be used in a later section where a theoretical prediction of the H_β radiation is made.

4955 Å Continuum Thermometry

The experimental value for the spectral intensity of the continuum at 4955 Å was obtained by linear interpolation between the 4550 and 5100 Å values obtained from the polychromator after subtraction of the H_β wings as explained in the preceding section. This was a small correction — between 1 and 9% of the polychromatic intensities.

The prediction was obtained in as direct a manner as possible from the work of Morris et al.[4] They tabulate, as a function of temperature and pressure, the continuum intensity of pure nitrogen at 4955 Å and that of pure oxygen at 4348 Å. These intensities were compared with the predictions obtained from our RATRAP code (see Ref. 1 for a description of this code) using FEMP composition data for both pure oxygen and pure nitrogen. The results are shown by Fig. 9 where it is noted that the Morris et al. values were higher. The RATRAP code as then modified by increasing the nitrogenic contributions by a factor of 1.11 and the oxygenic contributions by an amount $0.8 + 0.4(T/12,000\,\text{K})$. These factors are shown by the dotted lines of Fig. 9 and it is noted that they fit the ratios to within a few percent. Thus this modified RATRAP code would yield intensities for the pure gases that were very close to those of Morris et al.[4] It is felt that the values from this modified code for a mixture of
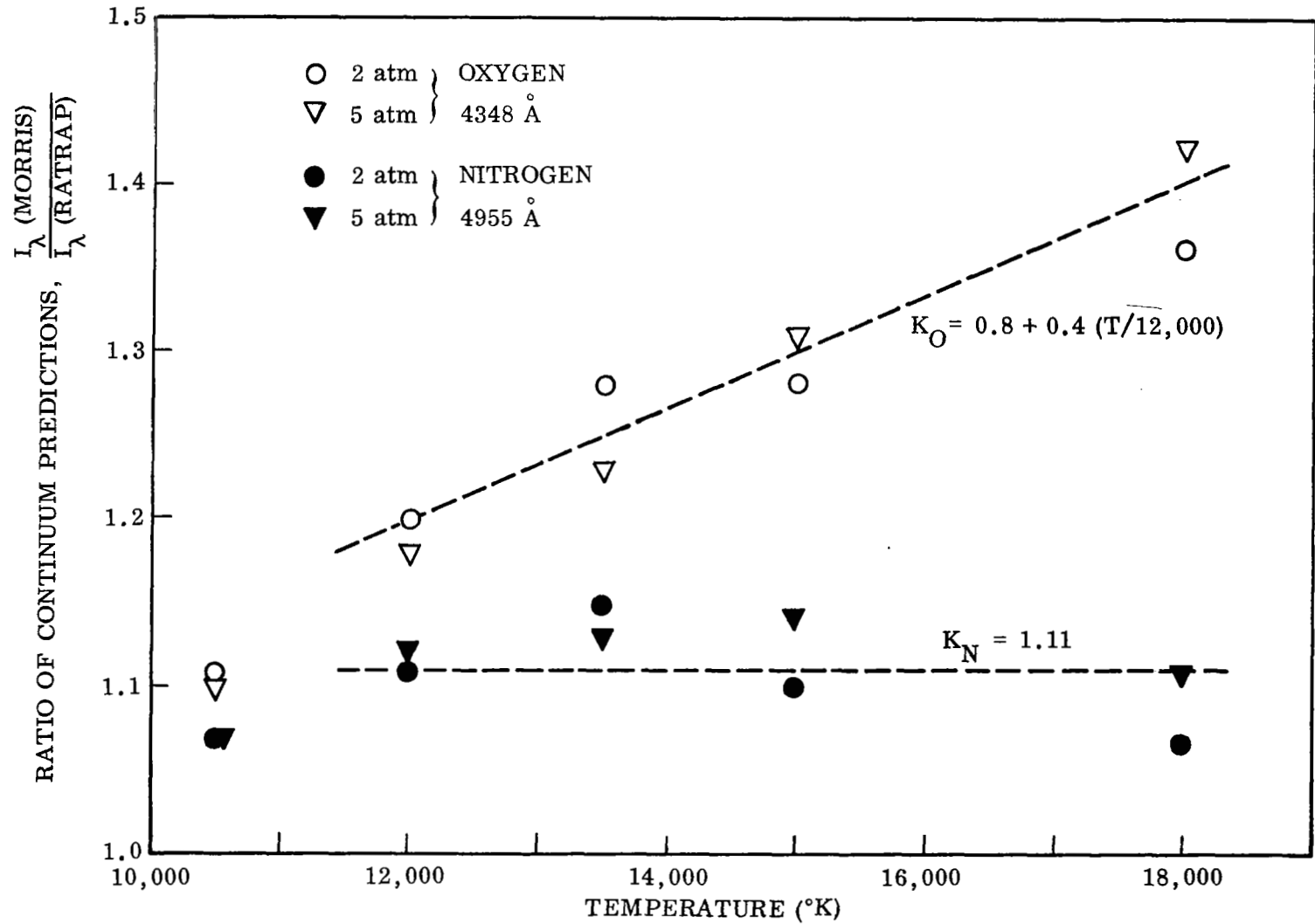
32

Fig. 9 Comparison of Continuum Predictions From Morris et Al. and Ratrap Code

these two gases at the wavelength of the principal constituent represent a reasonable application of their work. While this modification procedure did not involve the RATRAP predictions for pure hydrogen, its continuum is relatively weak and since the plasma contains only 10% hydrogen, possible errors from this source would have to be quite small.

Therefore the continuum spectral intensity predictions for air + 10% hydrogen at 4955 Å were obtained from this modified RATRAP code and the appropriate FEMP composition data. The results were scaled by $(P)^{1.3}$ and are shown for the two pathlengths of this experiment in Fig. 10 where the validity of this scaling can be assessed. To justify that no large errors were made in this procedure, it is noted that the lower solid curve is within ±3% of the Morris et al[4]. values for pure nitrogen at 5 atm when their tabulated values are multiplied by 8.5 (an optically thin pathlength), divided by 8.1 (the 5-atm pressure scaling), and then multiplied by 0.80. This last factor was obtained from the mole-fractions of the test gas by assuming that oxygen radiates half as much as nitrogen, and hydrogen negligibly little − a rough but not unreasonable approximation to locate large errors.

The error analysis to be considered in the next section will require an estimate of the accuracy of the curves of Fig. 10. For plasma thermometry, the continuum intensity can be considered as the means of transferring the plasma temperature diagnostic work of Morris et al[4] on their arcs to our plasmas. In this sense the validity of the continuum cross sections and attachment energies they obtained is of secondary importance because their conditions ($9 - 14,000\,°K$, $1 - 2$ atm) are close to ours. They determined their arc temperatures by measuring the integrated line intensity of well-
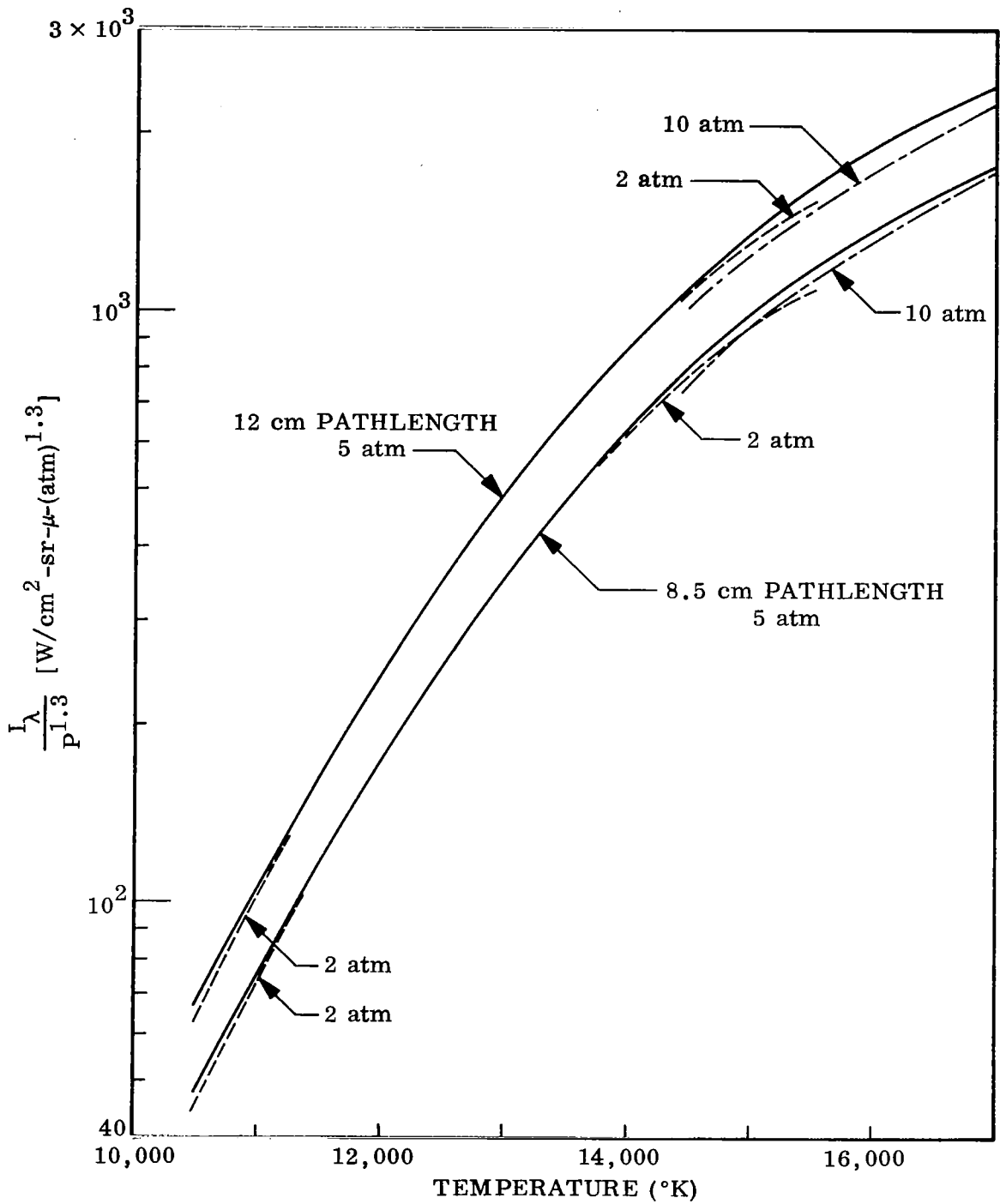
Fig. 10 Continuum Spectral Intensity Predictions at 4955 Å for Air + 10% H_2

known NI and OI lines. Assuming a ± 5% measurement using ± 10% f–numbers and an accurate pressure, it can be shown[2] that this technique is capable of yielding better than ± 1.5% temperatures for pure gases at their conditions. Actually their arcs were nonisothermal and their test gases not pure, but these are largely random effects which are of small consequence since they made repetitive measurements. Because they measured the continuum intensity with the same spectroscopic system at an adjacent wavelength, this better than 1.5% temperature uncertainty is equivalent to a ± 15% uncertainty in their tabulated values for the continuum intensity. The process of computing the curves of Fig. 10 included the effects of the imperfections in the modified RATRAP procedure, the wavelength change for oxygen, and the untested hydrogen contribution. These are estimated to be ± 5% and, in view of the symmetrical nature of the corrections shown in Fig. 9 and the close correspondence with the rough approximation made above, this will be treated as a random error. Thus, for use in the following error analysis, the curves of Fig. 10 are estimated to have ± 15% systematic errors and ± 5% random errors.

Error Analyses

In all three diagnostic techniques, a temperature was obtained from the measurement of a radiative quantity M which depended on the thermodynamic state and certain physical constants C. The functional relationship is M = f(T, P, C) and the total differential of M can be cast in the following form:

$$\frac{dT}{T} = \frac{\dfrac{dM}{M} - \dfrac{P}{M}\dfrac{\partial M}{\partial P}\bigg|_T \dfrac{dP}{P} - \dfrac{C}{M}\dfrac{\partial M}{\partial C}\bigg| \dfrac{dC}{C}}{\dfrac{T}{M}\dfrac{\partial M}{\partial T}\bigg|_P} \tag{8}$$

36

The left side represents the temperature uncertainty while the numerator on the right includes the uncertainty in the measurement of M together with the effect of an uncertain pressure and physical constants. During the following analyses, those portions of the numerator which represent possible systematic errors affecting the accuracy of the measurements will be separated from the random errors which affect the precision. This numerator is divided by the dimensionless partial derivative which is called the temperature sensitivity.

The measurement of the Planck function B_λ at the Hα wavelength is easily analyzed because it is not pressure dependent and the radiation constants may be considered as accurately known. Thus, for the Planck function, Eq. (8) becomes

$$\frac{dT}{T} = \frac{\dfrac{dB_\lambda}{B_\lambda}}{\dfrac{C_2}{\lambda T}\dfrac{\exp(C_2/\lambda T)}{\exp(C_2/\lambda T) - 1}} = \frac{(\pm 3\%)_{sys.} + (\pm 4\%)_{random}}{denominator} \tag{9}$$

where $C_2 = 1.439 \times 10^4 \,\mu K$ and, for Hα, $\lambda = 0.6563\,\mu$. The systematic errors are entirely those of the standard lamp — the calibration supplied with the lamp is stated by the manufacturer to be accurate to $\pm 2\%$ and this was increased to $\pm 3\%$ by the adoption of an often-compared working standard. The random errors, introduced by meter and oscilloscope calibrations, PM tube dynode voltage changes, etc., may be estimated by noting that the ratio of the two 6563 Å intensities varied between 0.96 and 1.08 during the course of this experiment. Since the two red PM tubes were operated completely independently and since their outputs were averaged to obtain a single intensity, the random error in the Hα intensity is estimated to be $\pm 3\%$. The correction for the nonblack regions near the slit edges was less than 10% of this

intensity and assuming that the correction was accurate to $\pm 10\%$ adds another $\pm 1\%$ to the random error. Thus the random errors are estimated to be $\pm 4\%$. The temperature sensitivity of Eq. (9) is evaluated in Fig. 11 and the resultant estimates of the systematic and random errors are shown in Figs. 12-A and 12-B, respectively.

For the measurement of the 4955 Å continuum intensity I_λ^c, Eq. (8) becomes

$$\frac{dT}{T} = \frac{\dfrac{dI_\lambda^c}{I_\lambda^c} - 1.3\,\dfrac{dP}{P} - \dfrac{dC}{C}}{\left.\dfrac{T}{I_\lambda^c}\dfrac{\partial I_\lambda^c}{\partial T}\right|_P} = \frac{(\pm 18\%)_{\text{sys.}} + (\pm 14\%)_{\text{random}}}{\text{denominator}} \tag{10}$$

where the coefficient of the pressure uncertainty was obtained from the scaling used in Fig. 10. The systematic errors of $\pm 18\%$ stem from the $\pm 15\%$ estimate of the accuracy of the curves of Fig. 10 as discussed in the previous section together with the $\pm 3\%$ accuracy of the working standard lamp as discussed above.

During the course of the experiment, the ratio of the corrected polychromatic continuum intensities at 4550 Å to those at 5100 Å varied between 1.02 and 1.16. (The extremes occurred at nearly the same plasma temperature.) Incidentally the modified RATRAP code predictions yielded ratios of $1.12 - 1.18$ and, while not to be taken literally, are regarded as encouraging evidence that no gross errors were present. The linear interpolation to 4955 Å was essentially an averaging process leading to an estimate of $\pm 4\%$ for this value. The less-than-10% H_β wing corrections, if done to only $\pm 10\%$, contribute another $\pm 1\%$. The $\pm 3\%$ pressure uncertainty contributes $\pm 4\%$ and the random errors associated with the computation of the curves of Fig. 10 were estimated to be $\pm 5\%$. Thus, the total random errors are estimated to be $\pm 14\%$.
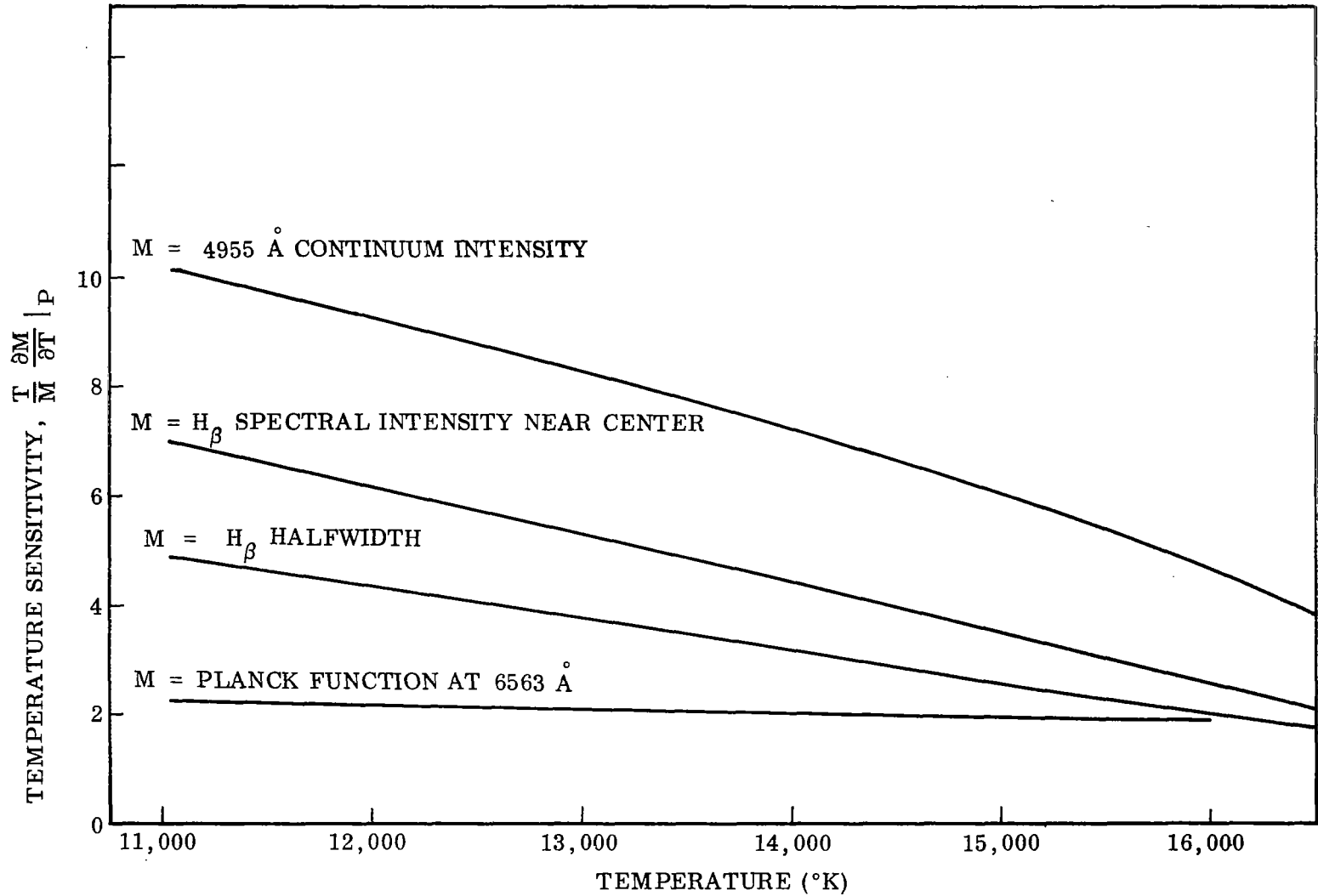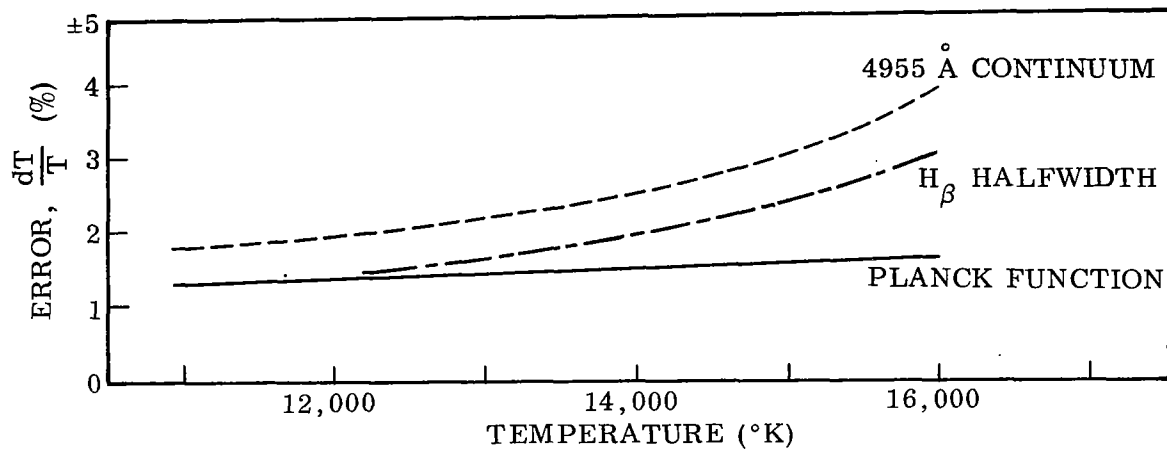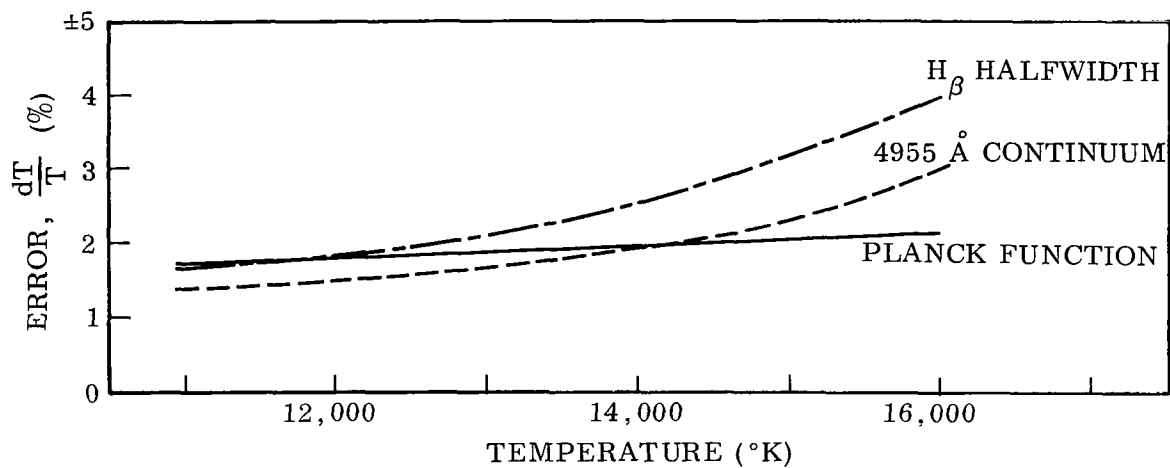
Fig. 11 Temperature Sensitivity of Diagnostic Techniques Evaluated Along the Hugoniot States

A. Systematic Errors

B. Random Errors

Fig. 12 Estimates of Systematic and Random Errors

The temperature sensitivity shown in Fig. 11 was obtained by numerical differentiation of the modified RATRAP code predictions and the resultant error estimates are shown in Fig. 12.

For the H_β shape measurement, the measured quantity was the averaged halfwidth $\overline{\gamma}$ given by Eq. (7) and temperature is introduced by the discussion of the electron density that followed. Thus Eq. (8) becomes

$$
\frac{dT}{T} = \frac{\dfrac{d\overline{\gamma}}{\overline{\gamma}} - 0.4\dfrac{dP}{P} - \dfrac{d\alpha_{1/2}}{\alpha_{1/2}}}{\dfrac{2}{3}\dfrac{T}{N_e}\left.\dfrac{\partial N_e}{\partial T}\right|_P} = \frac{(\pm 6\%)_{\text{sys.}} + (\pm 8\%)_{\text{random}}}{\text{denominator}} \tag{11}
$$

The systematic errors lie entirely in the validity of the constant $\alpha_{1/2}$ since it is not felt that our treatment of the asymmetries was significantly different from anyone else's. Kepple[8] reports that his H_β shapes (i. e., halfwidths) agree with experimental measurements to $\pm 4\%$ over electron densities of $2 \times 10^{16} - 2 \times 10^{17}$ cm^{-3} and $20,000°$K. However Shumaker and Popenoe[12] assert that only limited experimental tests have been performed above 8×10^{16} cm^{-3} and claim, on the basis of their work, that Kepple's widths are too wide by 7% at 2×10^{17} cm^{-3}. In a similar experiment, Morris and Krey[13] report that Kepple's widths are too wide by $3 - 5\%$ although they do not regard this as significant. Therefore a systematic uncertainty of $\pm 6\%$ is assigned to Kepple's value of $\alpha_{1/2}$ and we note here for use later that the -6% extreme might be more nearly the true value, at least at electron densities near 2×10^{17}.

The random errors include the $\pm 7\%$ halfwidth measurement discussed earlier while the $\pm 3\%$ pressure uncertainty contributes another $\pm 1\%$, making the total random

41

errors ± 8%. The temperature sensitivity was obtained from the FEMP tabulations and is plotted in Fig. 11; the resultant error estimates are plotted in Fig. 12.

The validity of all these error estimates will be assessed in the next chapter when the individual measurements are discussed.

Use of H_β Intensities

The measured intensity of the 19 Å central portion of H_β was not used as a primary diagnostic technique because it would not be in the same accuracy class as the three just discussed. Thermometry on a portion of a line shape is basically undesirable because it combines the uncertainties of both intensities and shapes and this is not compensated by an increase in the temperature sensitivity. Further, for H_β the theoretical shape near the center is none too good (although experimental shapes are available). Finally in the case at hand, the intensity directly involves the hydrogen number density — a dependence avoided in the shape of H_β and the intensity of optically thick $H\alpha$.

The H_β intensities were used to determine the nonsteady behavior and as a measure of the experimental concentration of hydrogen as discussed in the next chapter. Assuming (for simplicity only) that the H_β radiation was optically thin, the spectral intensity for a pathlength of δ (cm) is

$$I_\lambda(H_\beta) = 35.1\,\delta\exp\left(\frac{-12.8}{kT}\right)\frac{N_H}{(N_e)^{2/3}}\,S(\alpha) \quad , \quad \frac{W}{cm^2\,sr\,\mu} \qquad (12)$$

where $S(\alpha)$ is normally the shape parameter tabulated by Kepple[8]. However, for the problem at hand, this shape did not adequately represent the central portion of the line shape as indicated earlier by Figs. 6 and 7. Therefore, to represent the average

spectral intensity over the 19 Å exit slit, $S(\alpha)$ was taken to be the peak tabulated value multiplied by the experimentally obtained ratio $\overline{S}(\alpha)/S(\alpha)_{max}$ plotted in Fig. 8. This procedure was not strictly correct because the resultant hybrid shape was no longer normalized to unity, but the errors incurred were small because the central portion was a small fraction of the total shape and the theoretical shapes appeared to reasonably represent the experimental shapes from the maximum points out toward the wings. The temperature sensitivity of this intensity is given by

$$\frac{T}{I_\lambda} \frac{\partial I_\lambda}{\partial T}\bigg|_P = \frac{T}{N_H} \frac{\partial N_H}{\partial T}\bigg|_P - \frac{2}{3} \frac{T}{N_e} \frac{\partial N_e}{\partial T}\bigg|_P + \frac{12.8}{kT} \tag{13}$$

and is plotted in Fig. 11.

RESULTS

Nonsteady Behavior

The photoelectric traces from the polychromator and the zero-order trace from the spectrograph again[2] showed the marked similarity which was taken as experimental verification of the presence of chemical equilibrium. These traces did, however, generally show a linear decrease with time indicative of unsteady behavior. This is typified by Fig. 13 where it is apparent that the continuum channels decreased the most and the Planck function the least. However this is entirely consistent with the temperature sensitivities of these radiative quantities. (See Fig. 11.)

These decreases were systematized by dividing each slope (% change in M per unit time) by the appropriate temperature sensitivity (% change in M per % change in T) to yield the rate of temperature change. The results for all the traces obtained during this experiment are shown in Fig. 14. The two continuum and the two Planck function traces were each averaged — they did not differ substantially. The traces were linearized to the point where an obvious bump or dip signified the end of the test time. The temperature sensitivity of the H_β channel was appropriately weighted for the underlying continuum.

The most remarkable feature of Fig. 14 is the utter lack of any temperature dependence. This was entirely unexpected and must be taken as strong evidence that the temperature changes were not caused by radiative cooling because this would be strongly temperature dependent.
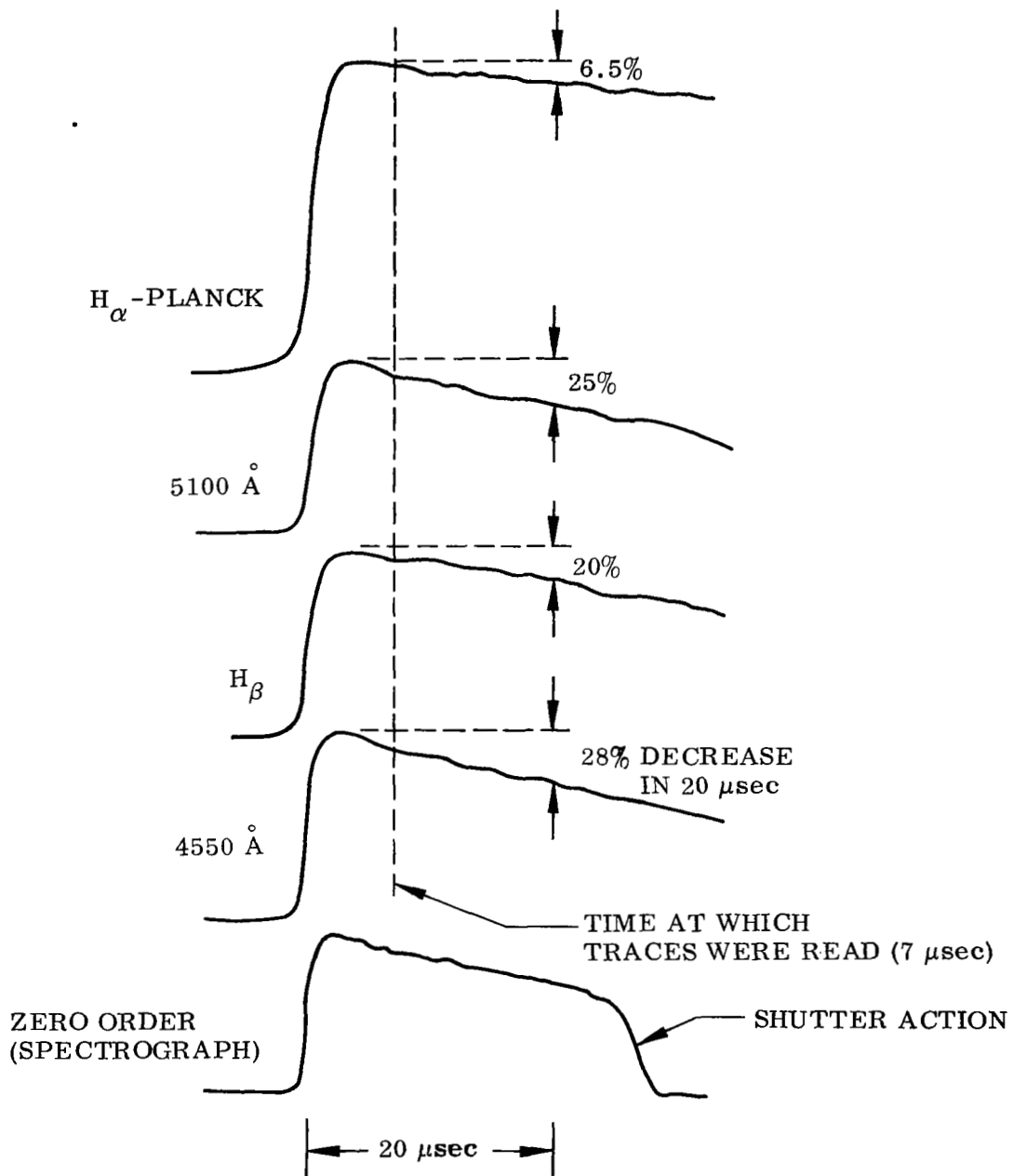
Fig. 13 Photoelectric Traces From Shot 630 (U_s = 9.51 mm/μsec)

45

Fig. 14 Time Rate of Temperature Change in Reflected Shock Region

From a thermometric standpoint the small magnitude of the ordinate is noteworthy. The data points average at a value of about $-0.1\%/\mu$sec corresponding to a relatively small 1% decrease in temperature over 10 μsec. The rate derived from the Planck junction is lowest on all but two shots (where it is close) while the H_β and continuum-derived rates tend to be quite similar. This is consistent with the experimental conditons. The large optical depth at $H\alpha$ made the Planck function sensitive to sidewall boundary layers while the optically thin conditions at H_β and especially the continuum made these measurements reflect bulk gas properties over the full 8.5- or 12-cm pathlength. The fact that these rates are as close as they are is important evidence that no appreciable absorption occurred in the sidewall boundary layer.

Since time-dependent changes were observed, it is appropriate to comment on where (in time) the results were based. The polychromatic traces were read about 7 μsec after passage of the reflected shock to correspond to an average over the 15 μsec measurement time in the cavity model used to obtain the total intensity results.[1] The exposure times in the spectrograph averaged about 22 μsec (min. 14, max. 28) and thus the H_β shapes represented a somewhat longer time-average than did the purely photoelectric measurements of the Planck function and the continuum intensity. However in light of the results of Fig. 14, the difference in temperature was negligibly small and no adjustment was made.

Results of Temperature Measurements

The first task of this section is to assess the quality of the results. The basis is the average of the three (only two in several cases) results from the three different thermometric techniques employed on each shot. The percentage deviations between

each result and this mean value are shown by Fig. 15. To assist this assessment, error bands representing the average of the systematic error estimates (Fig. 12-A) were also drawn.

Taken by themselves, the data scatter by less than ±3% which is testimony to the quality of the results. It is interesting to note that the error estimates (Fig. 12) would allow the data scatter to increase at the higher temperatures, but that such behavior was not realized in practice. While some systematic deviations are apparent, this behavior is largely within the limits of the error bands — the low-temperature H_β results being a possible exception. The two experiments which reported the halfwidths to be about 6% too wide[12, 13] were conducted at electron densities corresponding to about 13,000° K in Fig. 15. The temperature sensitivity here is about 4 so reducing Kepple's[8] values by 6% would raise the H_β temperatures 1.5% and make the agreement here look better. However this same correction, if applied uniformly, would raise the H_β results 3% at the high-temperature end and here they look good as they are. Since such a correction would represent an extrapolation to much higher electron densities where no similar data are available, it was decided to use Kepple's[8] values uniformly.

Such comments notwithstanding, the average systematic error bands enclose the majority of the data points and those outside are no farther than (and in most cases considerably within) the deviations allowed by the random error estimates of Fig. 12-B. Therefore these bands represent a liberal estimate of the accuracy of this experiment. In the figure to follow, the error bars represent the appropriate height of these bands. The plotted point — the mean measured temperature — represents
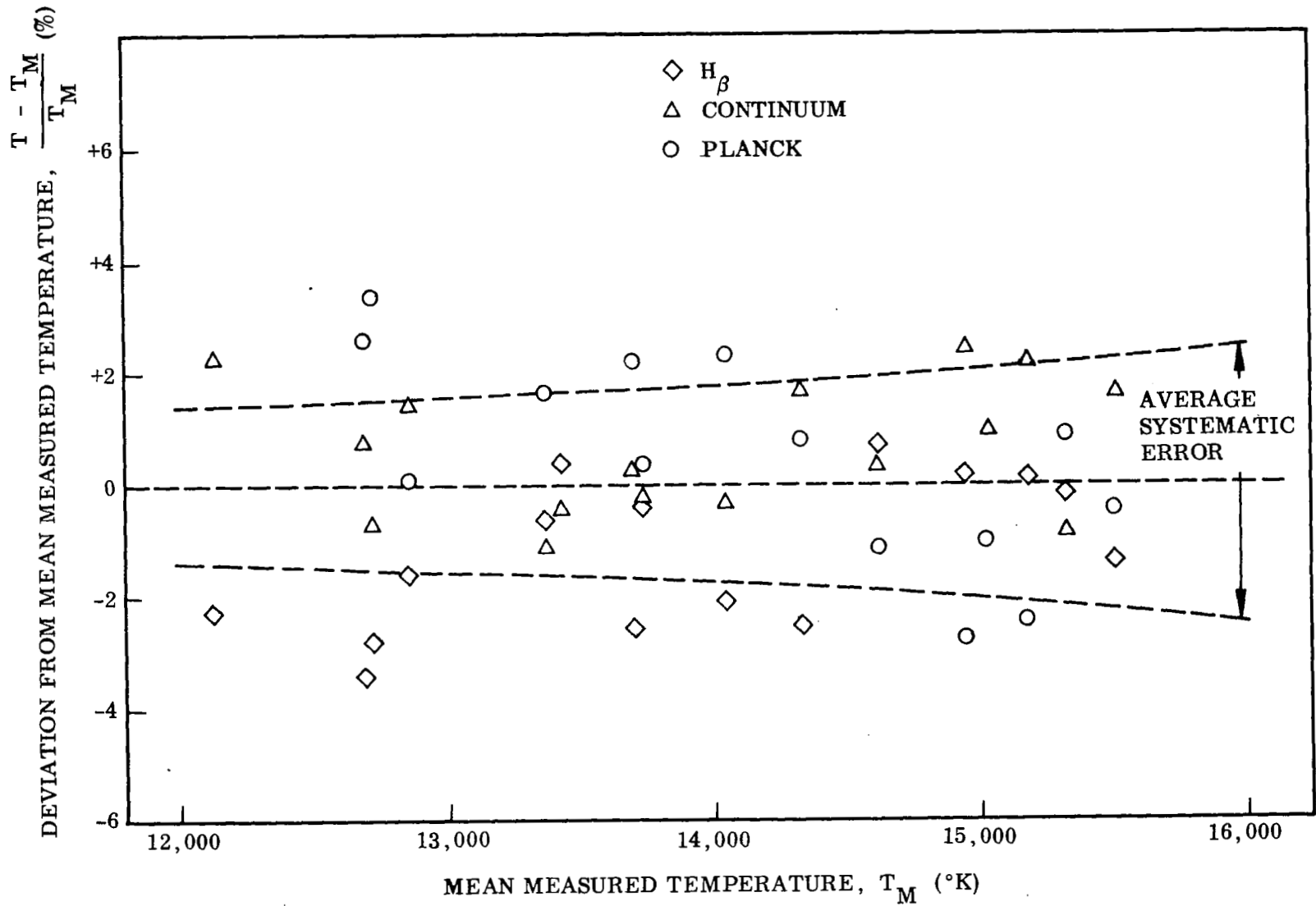
Fig. 15 Deviations Between Individual Results and Their Mean for Each Shot

the most probable value because the systematic errors in each technique stem from largely unrelated sources.

The principal objective of this research was to compare the measured temperatures with the gasdynamic temperatures and this comparison is presented by Fig. 16. Also included are the results obtained last year[2,3] with ± 2% error bars obtained by considerations similar to those above and with the deviations reduced by subtracting 0.35% to compensate for the lower initial pressure caused by the McLeod gauge calibration correction. Thus Fig. 16 contains all the thermometric results obtained during the whole research effort.

It is clear from Fig. 16 that the gasdynamic temperature was not realized on the bulk of the shots. Last year[2,3] it was remarked that the shock tube operation was erratic – shots with comparable incident shock speeds yielded measured temperatures that differed by almost 1000°K. To a lesser extent, this behavior persisted over the 12 – 14,000°K range while for the eight shots above 14,000°K, the shock tube acted quite repeatably and here regular deviations of 5 – 6% were encountered.

It is unfortunate that the shock tube did not behave more regularly so that the total radiation data[1] could be compared more accurately. Taken alone, the results from this year would appear to show a trend but this disappears when balanced against the earlier results. There is no reason to discount these earlier results which, in fact, represent averages of seven measurements employing three different techniques.

Since a temperature-dependent trend would be expected if radiative cooling were the loss mechanism, the lack of such a trend in the results of Fig. 16 would indicate that
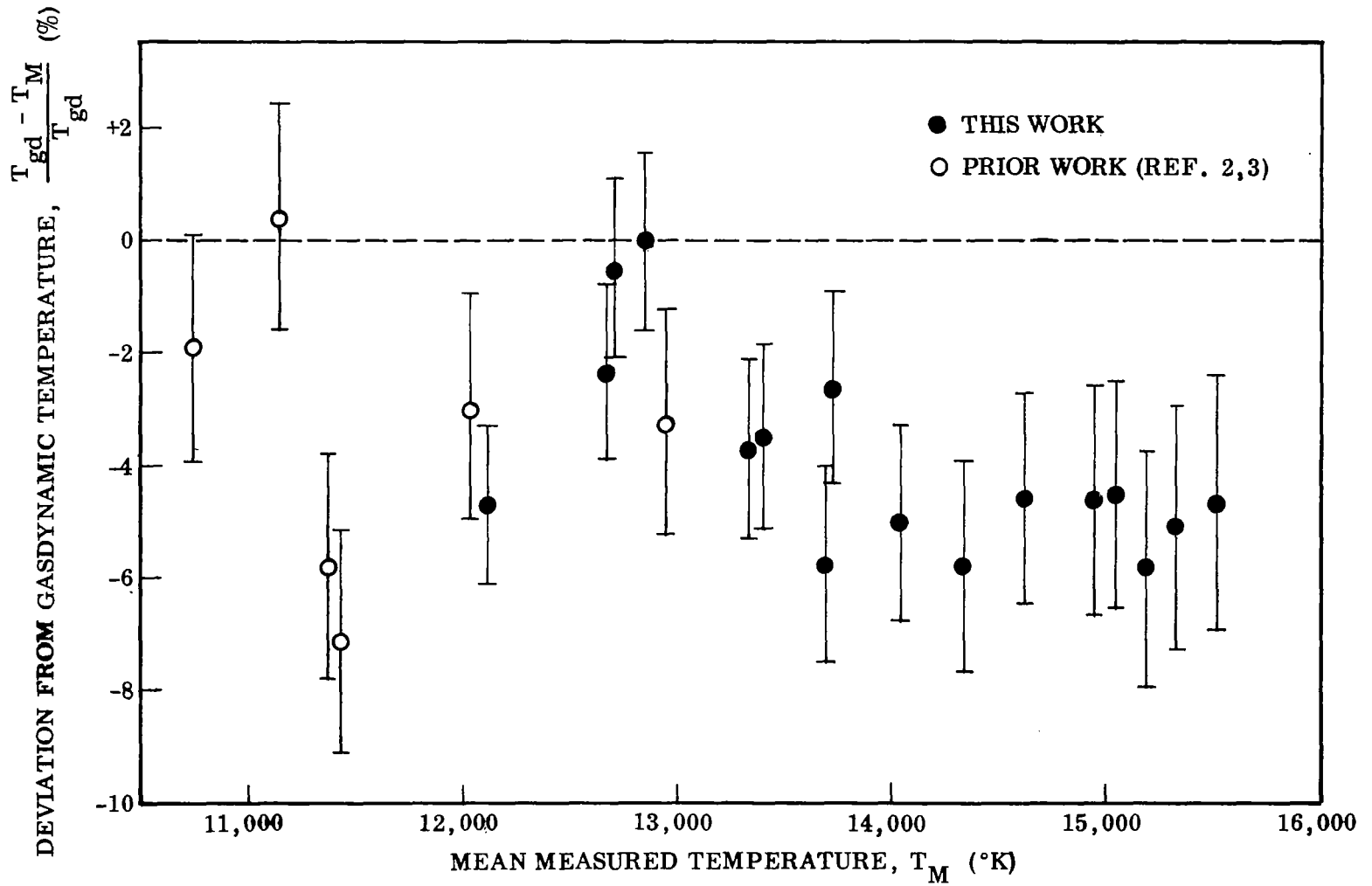
Fig. 16 Deviations Between Gasdynamic and Mean Measured Temperatures

radiative cooling was unimportant. This supports the conclusion derived from the rates of Fig. 14 where time-dependent changes and not absolute values were important.

Intensities of H_β

Figure 17 shows the polychromatic intensities for the 19 Å central portion of H_β obtained upon subtraction of the continuum level as determined by the 4550 and 5100 Å channels with opacity effects taken into account. Also shown are theoretical curves evaluated at both gasdynamic conditions (see Table 1) and at the same pressures but with temperatures reduced 5% below the gasdynamic values. These curves were obtained from a relation similar to Eq. (12) but with opacity effects included.

These curves are not intended to be used as primary thermometers — if they were, they would indicate temperatures 1.5 − 3% above those of Fig. 16. The intensity of H_β would make a relatively poor thermometer for reasons discussed earlier. Rather the curves should be considered as indication of a 10% systematic error which might well have been caused by the presence of 11% hydrogen rather than the assumed 10%. In retrospect this is not unreasonable since the hydrogen gas was admitted to the mixing container first and thorough mixing may not have occurred. Since neither the other hydrogen-derived diagnostics nor the gasdynamic temperatures depend strongly on the hydrogen concentration, an 11% hydrogen concentration would have very little effect on the results of this experiment.
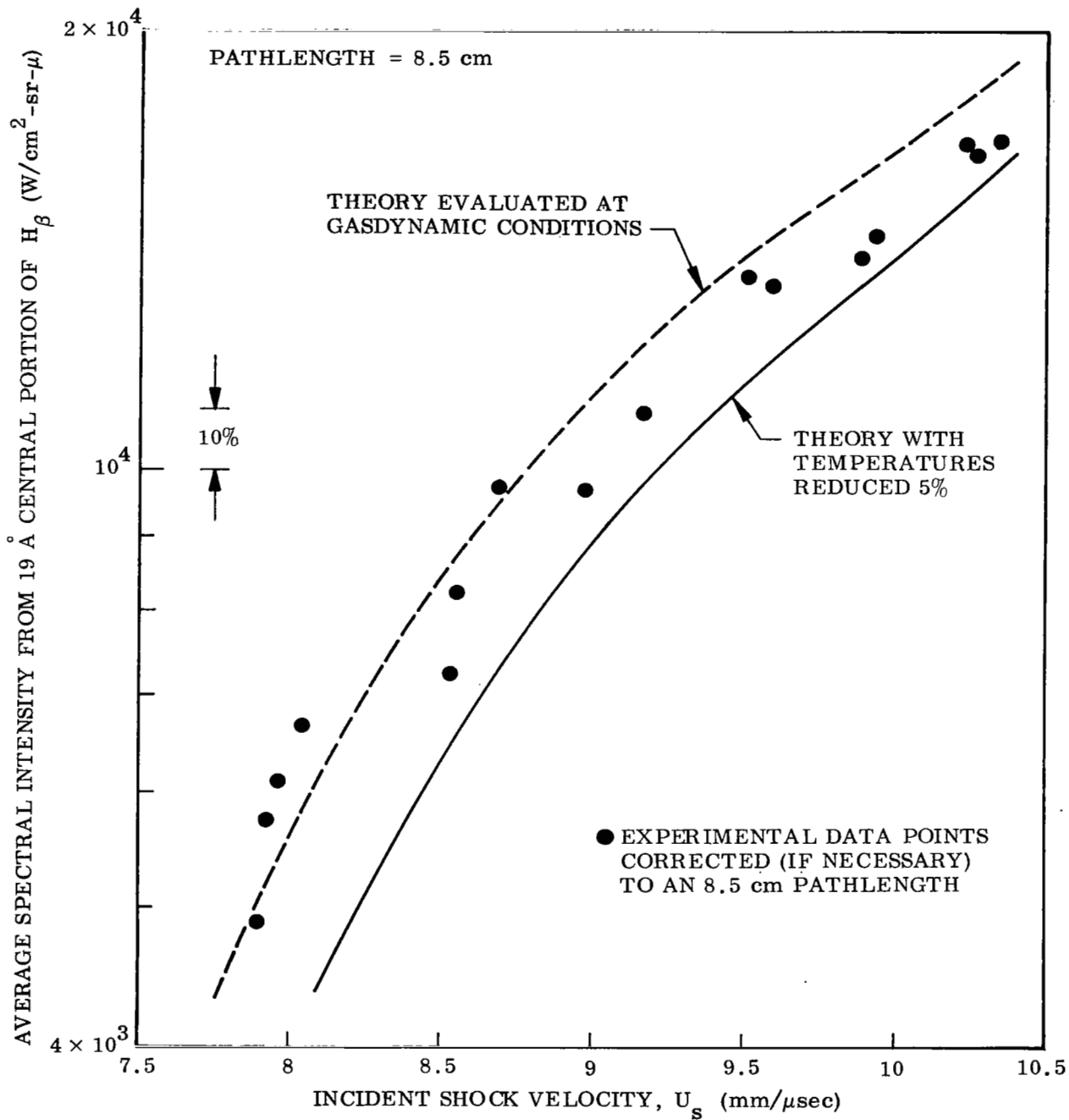
Fig. 17 Experimental Results and Theoretical Predictions for the Radiation From the Central Region of H_β
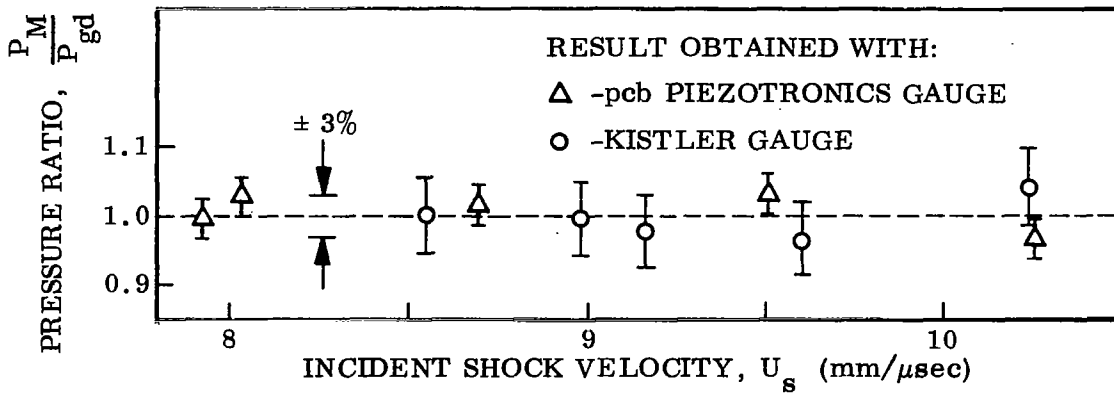
Endwall Pressure Results

Usable endwall pressures were obtained on 10 of the 16 shots and the results are shown in Fig. 18-A. The error bars represent the confidence level of each transducer and include uncertainties in both the calibration and the reading of the actual traces. It is clear from this figure that the measured values were within ±3% of the gasdynamic pressures. The symmetrical nature of the data scatter precludes any systematic errors and little, if any, significance should be attached to the ±3% scatter because of the difficulty in reading the gauge traces (see Fig. 4) with any greater precision. The error analyses of the preceding chapter showed that this small scatter did not appreciably affect the precision of the measured temperatures.
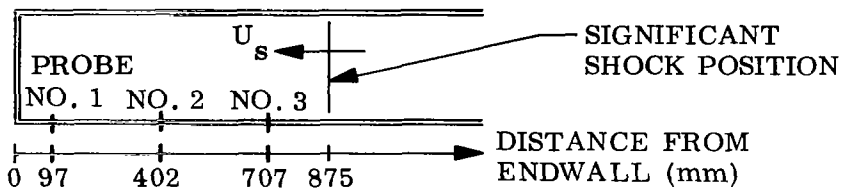
Incident Shock Velocity Measurement

This velocity was determined from time intervals measured between three ionization-type probes located 1 ft apart near the endwall as shown by Fig. 18-B. The outputs from adjacent probes were displayed as A minus B signals on oscilloscopes whose sweeps were calibrated by superimposing a 1-MHz sine wave from a crystal oscillator on the resultant oscillogram. The same operational mode was used – single sweep after a long wait. The time intervals were $30 - 40$ μsec and estimating that they could be read to the nearest 1/4 cycle of the sine wave yields an accuracy estimate of $\pm 0.4\%$ for the shock velocity. The two values so obtained were averaged to provide the basis for the gasdynamic properties used throughout this report.
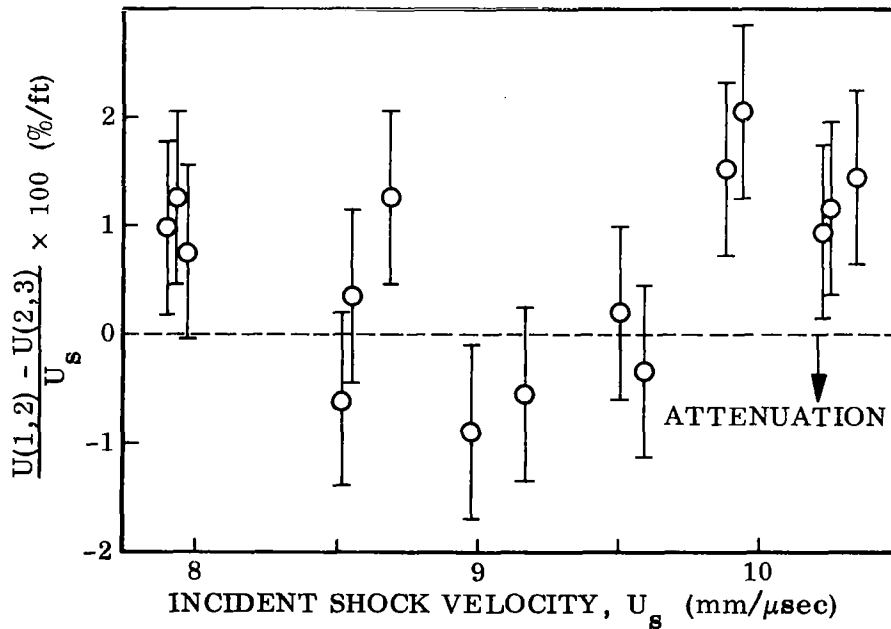
To make certain that these time intervals were meaningful, several experiments have been performed in the past. These involved installing pressure gauges either in place

A. Results of Endwall Pressure Measurement

B. Location of Ionization Probes

C. Incident Shock Velocity Change Near Endwall

Fig. 18 Endwall Pressure Results and Incident Shock Velocity Data

55

of or in addition to the ionization probes. The results have always indicated that the time intervals obtained from the ionization probes adequately represented those of the passage of the gasdynamic shock front.

The average velocity used for gasdynamic purposes represents the velocity at probe No. 2. The difference between the two velocities actually measured represents the change in a 1-ft interval and these differences are plotted in Fig. 18-C with ± 0.8% error bars to indicate the error doubling when differences are used. It is clear from this figure that the shock accelerated on about 3/4 of the shots and, for discussion purposes, the average change was an acceleration of about 0.6%/ft.

The overall density ratio (ρ_5/ρ_1) was about 125. (See Table 1.) Thus the test gas 7 mm from the endwall (where temperatures were measured) was processed by the incident shock when it was about 875 mm from the endwall — a location about 1.5 ft farther upstream than probe No. 2. The velocities at this point were, on the average, about 1% less than those at probe No. 2. It may be argued that the velocities at this upstream location would have been a more significant basis for the gasdynamic properties. This would lower the gasdynamic temperatures by 1.9% at 11,000°K, 1.2% at 13,000°K, and 0.8% at 15,000°K and hence reduce the deviations shown in Fig. 16 by these amounts. An effort was made to determine if a shot-by-shot correlation existed between the results of Fig. 16 and an individually applied correction for the shock speed. None could be determined since the corrections for the large-deviation points were about equally distributed between upward and downward revisions.

CONCLUSIONS AND RECOMMENDATIONS

This experiment successfully measured the thermodynamic properties of the test gas for temperatures up to nearly 16,000°K. The measured temperatures were about 5% below the gasdynamic values at temperatures above 13,000°K and varied erratically between 0 and 6 − 8% below at lower temperatures. No explanation was found for this erratic behavior. The accuracy of these measurements was about ±2% as predicted by the error analyses and as realized in the agreement obtained between measurements involving three different thermometric techniques. The endwall pressures were within ±3% of the gasdynamic pressures.

No significant evidence of radiative cooling was found since no temperature-dependent trends were evident in either the rates at which the test gas temperatures decreased or in the deviations between the measured and gasdynamic temperatures. No appreciable absorption occurred in the sidewall boundary layer since the optically thick Planck function rates and temperatures agreed with the results obtained from the other two diagnostic techniques at nearly optically thin conditions.

It may well be that the observed deviations from ideal shock tube behavior represent the total of many small effects. Three were found during this work. One, the shock accelerations, could lower the gasdynamic temperatures about 1% if the upstream shock velocity were used. Another was the less-than-1% increase in the measured temperatures that could be gained by correcting the measured temperatures for the observed rates of decrease. A third, caused by the apparent presence of an 11% hydrogen concentration rather than the assumed 10%, would lower the gasdynamic

temperatures by about 0.5%. Taken together, these three effects add to about 2% which leaves unexplained the largest part of the observed deviations from the gasdynamic temperatures. There may be other effects, although none were evident during this research.

Whatever the cause or causes of the observed behavior, the measured temperatures were obtained in a manner corresponding to the way in which the integrated intensity measurements were made several years ago.[1] Therefore the results of this experiment as shown by Fig. 16 may be applied directly to these measurements and this was the ultimate purpose of this research effort.

The results of the integrated intensity measurements are shown in Figs. 19 and 20. They were taken directly from a previous report[1] and, except for the theoretical predictions, the figures are identical. The predictions were obtained from a current RATRAP code which yields values that are somewhat lower than those from the version used previously. Besides several minor computational improvements, the major changes in the current code were the correction of a numerical error in the ionization potentials of NI and OI and a limiting of the effective shifts of the photoionization edges to 0.2 eV. Previously the shifts exceeded this value at high electron densities and this meant that the contribution from high-lying visible-IR lines was included twice. These changes result in predictions that are 15 − 20% lower in the window spectral region and 10 − 20% lower for the total spectrum.

In addition, the 8% calibration correction for the McLeod gage used to determine the initial tube pressure, which was only recently discovered, lowered the pressure used
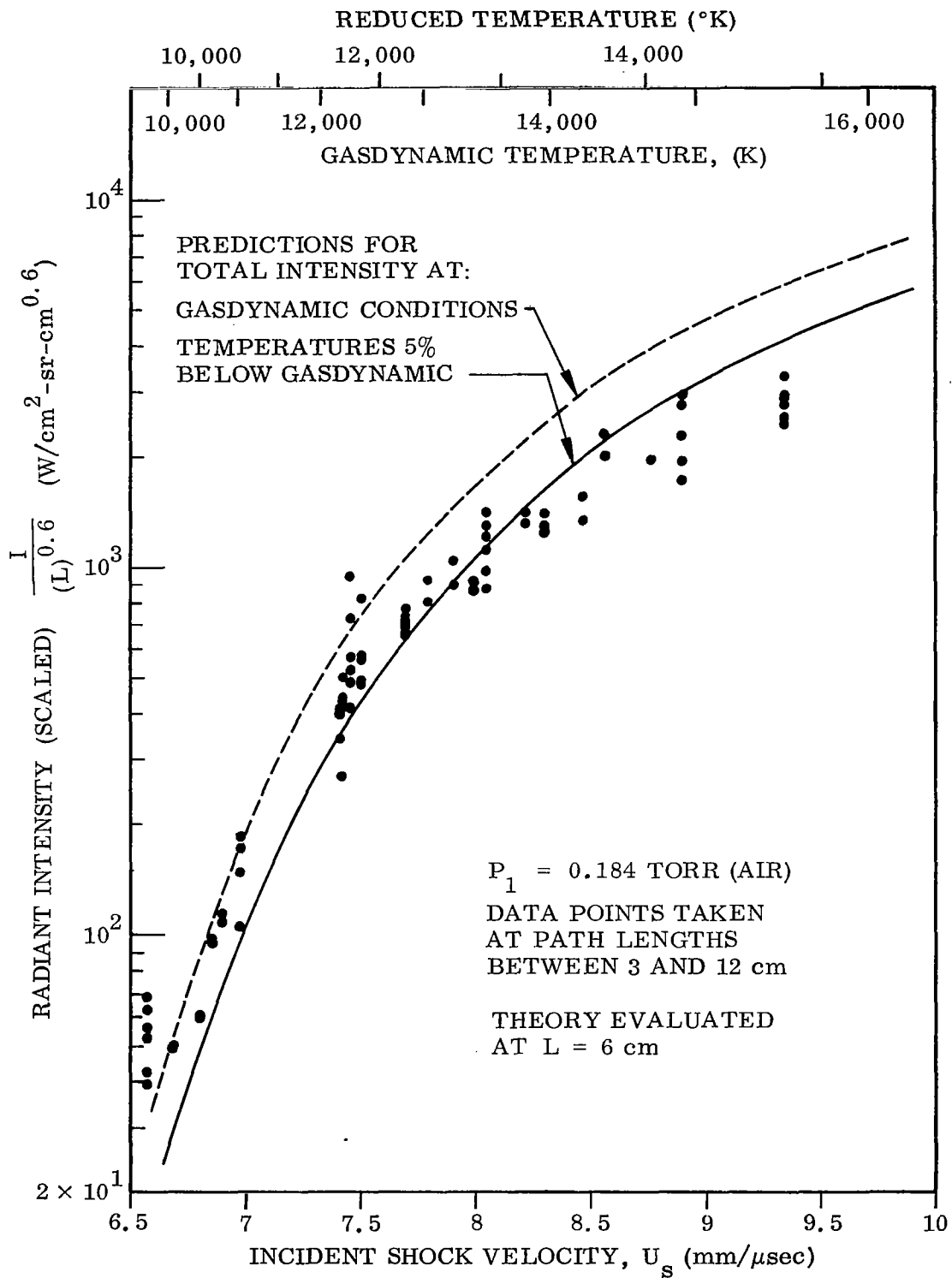
Fig. 19 Experimental Results for the Total Radiant Intensity and
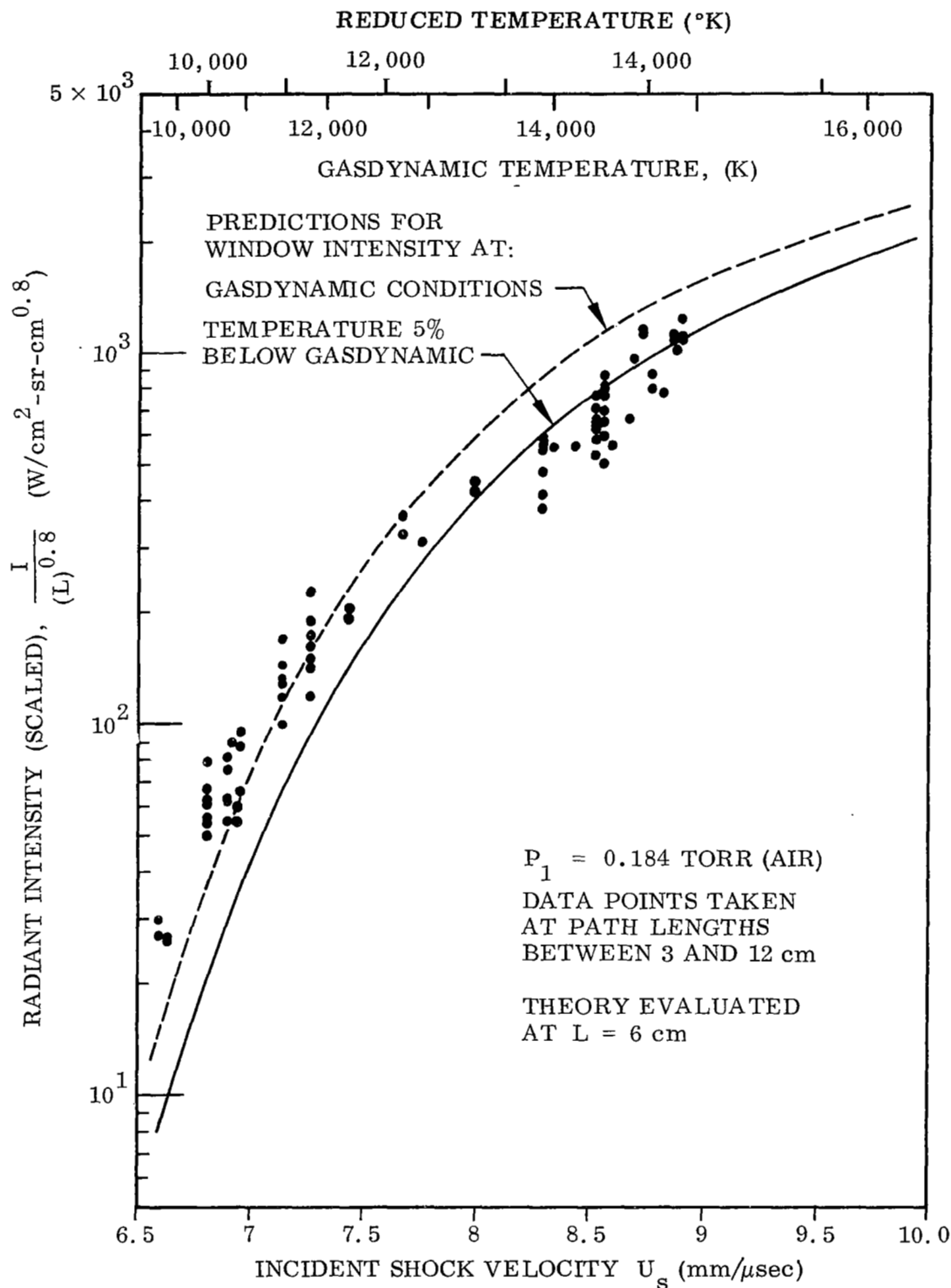Theoretical Predictions Evaluated at Both Gasdynamic
and Reduced Conditions

Fig. 20 Experimental Results for the Radiant Intensity Transmitted by a Quartz Window and Theoretical Predictions Evaluated at Both Gasdynamic and Reduced Conditions

in the predictions by 8%. This in turn lowered the window predictions by an additional 10% and the total predictions by 7%.

Thus, the dotted curves in Figs. 19 and 20 represent the predictions from the current RATRAP code at the gasdynamic conditions corresponding to a revised initial pressure of 0.184 Torr. The solid curves represent the predictions evaluated at the gasdynamic pressures but with the temperatures reduced by 5% to correspond approximately to the property values measured during this experiment. These latter predictions are about $30-45\%$ below those at the gasdynamic conditions.

The validity of lowering the gasdynamic temperature a uniform 5% may be assessed from the results shown by Fig. 16. Above about 13,000°K ($U_s = 8.2$ mm/μsec for air), the temperatures were fairly uniformly about 5% below gasdynamic so the correspondence is good. Below this, the measured temperatures scattered between 0 and $6-8\%$ low and so the data points, if the predictions are accurate, would be expected to fall between the curves or slightly below the lower curve.

The comparison of the total intensity results and these predictions shown by Fig. 19 yields almost exactly the behavior expected as the result of this correspondence for temperatures below 13,000° K except for one shot — the slowest — that lies entirely above the prediction at the gasdynamic conditions. It is noted that this condition is about 1000° K below the lowest measured temperature. At temperatures above ~13,000°K, the experimental results lie about 25% below the lower prediction and it is noted that here the measured temperatures were quite repeatable. (See Fig. 16.)

The corresponding comparison for that portion of the total intensity transmitted by a quartz window (Fig. 20) indicates that at the lower temperatures the experimental

results lie about 25% above the upper curve rather than between the two curves as might be expected by the nature of the measured temperatures. At intermediate temperatures the agreement is quite good, while at the higher temperatures the results scatter slightly below the lower prediction rather than around it.

On balance, the agreement between experiment and theory is much better than the former factor-of-two[1] which resulted from basing the predictions solely on the gasdynamic property values. Both predictions appear to be somewhat high at high temperatures while the window prediction appears somewhat low at low temperatures. Otherwise the agreement is quite good and even the disagreements are no worse than about 25%. This good correspondence between theory and experiment came only as the result of a 2-year effort to measure the actual thermodynamic conditions in the reflected shock plasma. Our confidence in these predictions is greatly increased because they no longer need be compared using assumed property values.

For future radiative measurements in shock tubes, it is strongly recommended that the researcher take heed of the above paragraph and perform simultaneous plasma-diagnostic measurements. The gasdynamic temperature is not sufficiently accurate to be used when measuring radiative quantities which vary as temperature to powers as high as 12, nor, at least in this experiment, was it repeatable. This same high sensitivity to temperature, which requires that temperatures be measured, can be used to advantage when determining temperatures through measurements of known radiative quantities.

The plasma diagnostic techniques used in the previous work[2,3] are applicable when the plasma conditions are such that the radiation from neutral atomic lines is

prominent. The techniques used herein are applicable at higher temperatures when this is no longer so. Finally at still higher temperatures, ion lines will become prominent and will make excellent thermometers. This experiment did not quite achieve high enough temperatures to make the ion lines measurable with sufficient accuracy. Calculations indicated that the peak spectral intensity of the strong NII^3 multiplet (5680 Å) would equal the continuum at 16,000° K, but the narrow width of the lines ($\gamma = 0.56$ Å at $N_e = 8 \times 10^{17}$ cm^{-3}) meant that this intensity would be reduced by instrument-function broadening and that still higher temperatures would be required.

Finally, the simultaneous use of different diagnostic techniques requiring different experimental assumptions and techniques lends credence to the accuracy of the resultant measurements.

REFERENCES

1. Wood, Allen D., Hoshizaki, Hiroshi, Andrews, J. C., and Wilson, K. H., "Measurements of the Total Radiant Intensity of Air," <u>AIAA J.</u> 7, 1 (Jan 69), 130 − 139.

2. Wood, Allen D. and Wilson, Kenneth H., <u>Radiant Energy Transfer Measurements in Air</u>, NASA Contractor Report CR-1390 (Oct 69).

3. Wood, Allen D. and Wilson, K. H., <u>Temperature Measurements of Air Plasmas in the Reflected Shock Region</u>, 7th Intl. Shock Tube Symposium, Toronto, Canada (Jun 69).

4. Morris, J. C., Krey, R. U., and Bach, G. R., "The Continuum Radiation of Oxygen and Nitrogen for Use in Plasma Temperature Determination," <u>JQSRT</u> 6 (1966), 727 − 740.

5. Gilmore, F. R., <u>Thermal Radiation Phenomena, Vol. 1 − The Equilibrium Thermodynamic Properties of High-Temperature Air</u>, DASA 1917-1, Vol. 1 (May 67).

6. McBride, B. J., NASA-Lewis, Private communication (via NASA-Marshall), 1967.

7. Hilsenrath, J. and Beckett, C. W., <u>Equilibrium Compositions and Thermodynamic Properties of Argon-Free Air</u>, Addendum to AEDC-TN-56-12 (1956).

8. Kepple, Paul C., <u>Improved Stark Profile Calculations for the First Four Members of the Hydrogen Lyman and Balmer Series</u>, Univ. of Maryland Tech. Report No. 831 (1968).

9. Kitaeva, V. F. and Sobolev, N. N., <u>Broadening of the Hydrogen Lines From Arc Plasma and Shock Tubes</u>, Soviet Physics — Doklady 6,4 (1961), 328 — 331.

10. Griem, H. R., <u>Plasma Spectroscopy</u>, McGraw-Hill, San Francisco, 1964.

11. Hill, R. A., Sandia Corp., Private communication (Jun 69).

12. Shumaker, J. B., Jr., and Popenoe, C. H., Experimental Test of H_β Stark-Broadening Theory at High Electron Densities, <u>Phys. Rev. Letters</u> 21,15 (7 Oct 68), 1046 — 1048.

13. Morris, J. C. and Krey, R. U., "Experimental Test of H_β Stark-Broadening Theory at High Electron Densities," <u>Phys. Rev. Letters</u> 21, 15 (7 Oct 68), 1043 — 1045.